TEKTONIKA

Constraining the 3-D Geometry of Fold-Thrust Belts Using Section Balancing vs. 3-D Interpolative Structural and Probabilistic Modeling

Kevin A. Frings [1,2], Christoph von Hagke [*2], Florian Wellmann [3], Elisa Heim [3], Miguel de la Varga [4], Hugo Ortner [5], Elco Luijendijk [6]

[1]Geological Institute, RWTH Aachen University, Aachen, 52062, Germany | [2]Department of Environment and Biodiversity, Division of Geology & Physical Geography, Salzburg University PLUS, Salzburg, 5020, Austria | [3]Institute for Computational Geoscience, Geothermics and Reservoir Geophysics (CGGR), RWTH Aachen University, Aachen, 52074, Germany | [4]Terranigma Solutions GmbH, Aachen, 52062, Germany | [5]Institute of Geology, University of Innsbruck, Innsbruck, 6020, Austria | [6]Department of Earth Science, University of Bergen, Bergen, 5020, Norway

Abstract Quantitative uncertainty analysis, 2-D and 3-D modeling of the subsurface, as well as their visualization form the basis for decision making in exploration, nuclear waste storage and seismic hazard assessment. Methods such as cross-section balancing are well established and yield plausible kinematic scenarios. However, they are based on geological data with errors and subject to human biases. Additionally, kinematic models do not provide a quantitative measure of the uncertainty of structures at depth. New 3-D modeling approaches have emerged that use computational interpolation, which are less dependent on human biases. Probabilistic extensions enable the quantification of uncertainties for the modeled structures. However, these approaches do not provide information on the time evolution of structures. Here, we compare classical cross-section balancing (2-D, kinematic modeling) with 3-D computational modeling to pave the way towards a solution that can bridge between these approaches. We show the strengths and weaknesses of both approaches, highlighting areas where probabilistic modeling can possibly add quantitative structural uncertainty information to improve section balancing. On the other hand, we show where probabilistic modeling still falls short of being able to cover the observed geometric complexities. We ultimately discuss how a workflow that iteratively combines results of the approaches can improve structural and kinematic constraints. As an example, we use the fold-and-thrust belt of the northern Alpine Foreland, the so-called Subalpine Molasse, focusing on the Hausham Syncline (Bavaria) and adjacent areas. We take advantage of the fact that here the stratigraphy as well as the tectonic history are well constrained. We show that shortening within the syncline progressively increases from west to east, independent from structural uncertainties. Two equally viable models can explain this. First, strain in the west is accommodated underneath the syncline in a triangle zone that progressively tapers out, or second, the strain difference is accommodated in more internal units. This highlights the importance of introducing uncertainty modeling also in kinematic restorations, as it enables identifying key regions, where different hypotheses can be tested.

Executive Editor:
Robin Lacassin
Associate Editors:
Adam Forte
Laura Federico
Technical Editor:
Mohamed Gouiza

Reviewers:
F. Robledo Carvajal
Nathan Eichelberger

Submitted:
8 September 2022
Accepted:
13 July 2023
Published:
15 September 2023

1 Introduction

Geological surface data, borehole and seismic data form the cornerstone of structural subsurface interpretations. Based on such data, geological models ranging from steady state geometric, kinematic to mechanical models can be derived. Geometric models may range from relatively simple conceptual sketches to 3-D models where individual surfaces are interpolated and visualized. For the latter, a multitude of methods, partly implemented in commercial systems, exists, which are tailored for generic or specific geological questions (*Wellmann and Caumon*, 2018). These solutions have in common that they yield geometric models of relevant structural features in the subsurface, satisfying all existing data from maps, boreholes and seismic sections. These models represent the present or steady state geometry of a geological system and hence only provide limited information on kinematic plausibility or time evolution. To address these aspects, the classic approach is section balancing (e.g., *Dahlstrom*, 1969; *Boyer and Elliott*, 1982; *Woodward et al.*, 1989; *Suppe and Chang*, 1983; *Gibbs*, 1983). This approach has been successfully applied to fold-thrust belts, entire orogens or

*✉ christoph.vonhagke@plus.ac.at

extensional systems (e.g., *Burkhard and Sommaruga*, 1998; *von Hagke et al.*, 2014; *Coward and Butler*, 1985; *Schmitz*, 1994; *Oncken et al.*, 1999). However, section balancing does commonly not include a full appreciation of the potential errors associated with interpretation of the data, and the predictive power of such models hinges on quality and density of the available data (e.g., *Kley and Monaldi*, 1998). Moreover, models are the result of the interpretation of individual geologists (e.g., *Oncken et al.*, 2006; *von Hagke and Malz*, 2018), and a much greater range of solutions may exist (*Butler et al.*, 2018). Suggestions have been made on how to analyze uncertainties in balanced sections (e.g., *Judge and Allmendinger*, 2011), and it has been shown that quantifying these uncertainties remains challenging (*Witte and Oncken*, 2020). Furthermore, the existence of conceptual bias in interpretations of the subsurface has been analyzed statistically (*Bond et al.*, 2007; *Schaaf and Bond*, 2019), and strategies exist how to reduce confirmation bias (*Wilson et al.*, 2019). However, despite the promising avenues standard models commonly do not include a quantitative estimate of the uncertainty of structures at depth (e.g., *Turner*, 2006). This is partly because we lack tools to model uncertainties in steady-state models, which then further complicates extending uncertainty estimates to kinematic models.

In this study, we apply kinematic as well as steady state uncertainty modeling to an example from the Alpine foreland fold and thrust belt, the Subalpine Molasse. The Subalpine Molasse is ideally suited to test and combine the different modeling approaches, as it is one of the best-studied foreland fold-and-thrust belts in the world. Similar structural and stratigraphic complexity as observed here can be expected in other foreland fold and thrust belts. We take advantage of the large existing data set in order to show strengths and weaknesses of the different modeling approaches, ultimately paving the way towards a combination of both, where geometric uncertainty can be implemented into kinematic models.

2 Previous Efforts in Uncertainty Modeling

During the last decades, the field of steady-state geometric 3-D modeling evolved from tools that initially focused on visualization to many novel approaches that now enable the consideration of geological models as scientific tools (see, for example, *Wellmann and Caumon*, 2018, for a recent review). In the context of this work, surface-based geometric representations take a central role. These methods evolved from interlocking triangular surfaces (*Jessell*, 2001), driven by 3-D CAD systems (*Mallet*, 1992; *Mayoraz et al.*, 1992; *Tipper*, 1992), to implicit surface representations (e.g., *Lajaunie et al.*, 1997; *Mallet*, 2004). Multiple methods have been proposed to obtain suitable surface representation schemes, for example based on co-kriging of surface contact points and orientations (*Lajaunie et al.*, 1997), discrete smooth interpolation (Mallet, 2004), radial basis functions (*Hillier et al.*, 2014), fold frameworks (*Laurent et al.*, 2016) and, more recently, also using machine learning approaches to evaluate hyperparameters (Gonçalves et al., 2017) and Graph Neural Networks for more flexible interpolation and the consideration of heterogeneous data sets *Hillier et al.* (2021).

One important focus of these developments has also been on methods to estimate uncertainties of the geological structures (e.g., *Wellmann et al.*, 2010; *Jessell et al.*, 2010; *Wellmann et al.*, 2014; *de la Varga and Wellmann*, 2016; *Schneeberger et al.*, 2017; *Wellmann et al.*, 2018; *Ailleres et al.*, 2019; *Brisson et al.*, 2023). These models provide an estimate of the plausibility of different geometric steady state models of the subsurface. In addition, several methods have been proposed to analyze and communicate these estimated uncertainties (*Wellmann and Regenauer-Lieb*, 2012; *Lindsay et al.*, 2012; *Lindsay et al.*, 2013). A recent study focusing on the triangle zone at the leading edge of deformation of the Subalpine Molasse has shown that uncertainty modeling of structurally and stratigraphically complex areas such as the Subalpine Molasse is possible (*Brisson et al.*, 2023). This study also indicates that including new constraints from kinematic data may help reducing uncertainty of geometric models. So far, aspects of geological evolution, as considered in kinematic models and cross-section balancing, are only considered to a limited degree (e.g., *Laurent et al.*, 2016; *Thiele et al.*, 2016). In the following, we will first provide a brief background of the geological history of the Subalpine Molasse and the study area. A more detailed description, including stratigraphy, can be found in the supplementary material. We will then present kinematic reconstructions before showing 3-D and probabilistic models. We will end with a discussion on how these approaches may benefit from each other paving the way towards a more complete integration of geometric, kinematic and probabilistic modeling.

3 Geological Setting

3.1 Stratigraphic Framework

The evolution of the Northern Alpine Foreland Basin (Molasse Basin) began in Cenozoic times with the closure of the Penninic Ocean that separated the European and Adriatic continental plates (e.g., *Frisch*, 1979; *Pfiffner*, 1986). The foreland basin sedimentary sequence was deposited on top of Mesozoic margin carbonates and hemipelagic muds derived from the passive European margin (Helvetic units) (e.g., *Freudenberger and Schwerd*, 1996). It consists of flysch to molasse successions that were deposited in the flexural basin (*Sinclair*, 1997a) including the Cretaceous Rhenodanubian Flysch (e.g., *Hesse*, 1982)

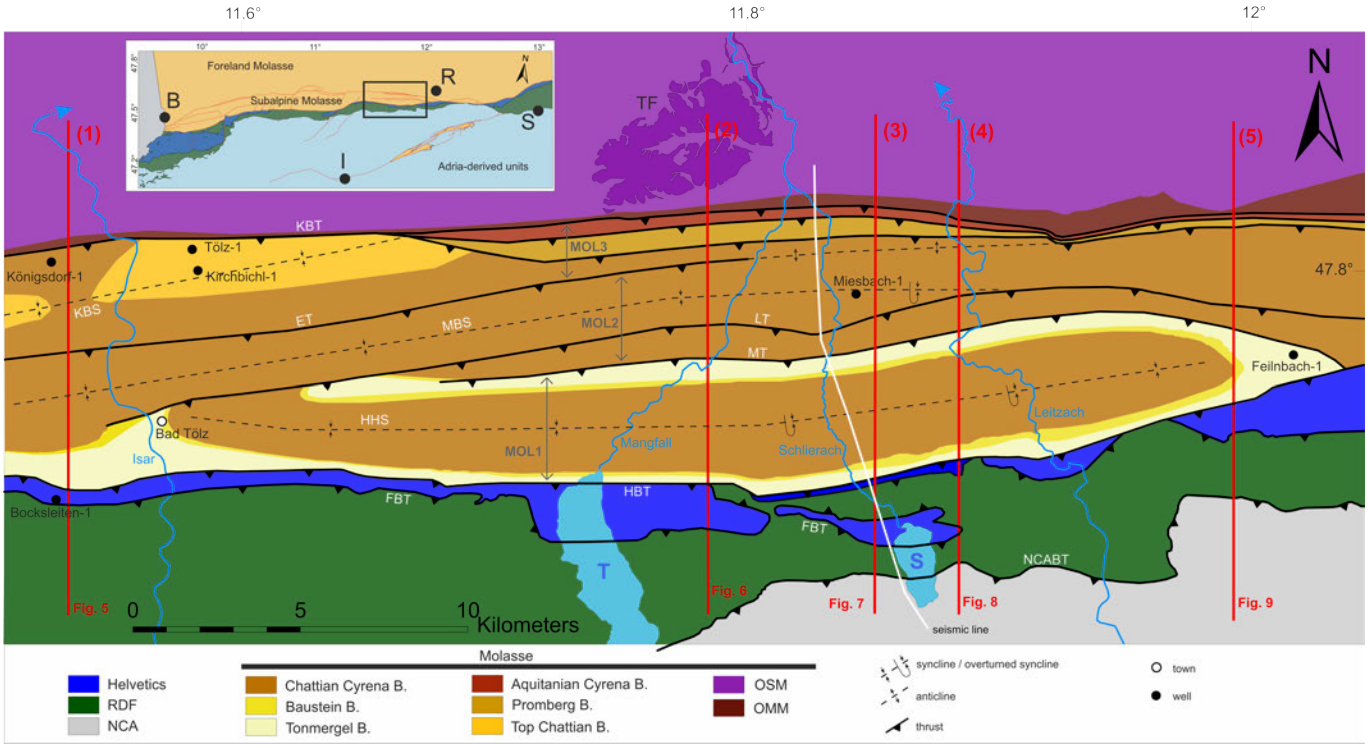

Figure 1 – Tectonostratigraphic map of the Hausham Syncline area, covering the Northern Calcareous Alps (NCA), Rhenodanubian Flysch (RDF) and the Helvetics, as well as the tectonic slices MOL1 – MOL3 of the Subalpine Molasse. Modified from *Ortner et al.* (2015). OMM denotes Upper Marine Molasse, OSM denotes Upper Freshwater Molasse. The thrust bounding tectonic units are called Northern Calcareous Alps Boundary Thrust (NCABT), Flysch Boundary Thrust (FBT), Helvetics Boundary Thrust (HBT), Mühlau Thrust (MT), Leitzach Thrust (LT), Ellbach Thrust (ET) and Kirchbichl Thrust (KBT). Fold axes traces are indicated for the Hausham Syncline (HHS), Miesbach Syncline (MBS) and Kirchbichl Syncline (KBS). North of the Subalpine Molasse, the Taubenberg Fan (TF) is located. Wells used in this study are labelled. Traces of the cross-sections (1) – (5) are marked. Inset map shows an overview of the study area location at the northern front of the Alps (black box). B: Basel; R: Rosenheim; I: Innsbruck; S: Salzburg (modified from *Ortner et al.*, 2015).

and the Molasse of Rupelian and younger ages (*Sinclair*, 1997b). Stratigraphy shows variability along strike the orogen and locally complex mechanical stratigraphy (e.g., *Ortner et al.*, 2023). Our study area is located between the rivers Isar and Inn, extending over forty kilometers in W-E direction (Figure 1). From north to south, the area extends from the flat-lying Molasse through the Subalpine Molasse and the Helvetic Units into the Rhenodanubian Flysch. Building a steady state geological model requires establishing a consistent stratigraphy throughout the entire study area. To this end, all existing stratigraphic data were compiled, and time- and facies-equivalent horizons were synthesized for all tectonostratigraphic units (Figure 2). Stratigraphic complexity within the Molasse deposits exists at all scales as during most of the time of deposition the area marks the facies transition zone from terrestrial environments (west) to marine environments (east), related to two regressive megacycles (e.g., *Paulus*, 1963; *Kuhlemann and Kempf*, 2002). Important marker horizons are the Rupelian Tonmergel Beds and the Lower Chattian Baustein Beds, which can be traced through the entire study area. These can be used as marker horizons for synthesizing the sometimes very local stratigraphic subdivisions into one consistent column. Another important stratigraphic unit that can be used for that purpose is the Lower Chattian Coal Formation. A review of the local stratigraphic complexity and how we built the stratigraphic column for our modeling approach can be found in the Supplementary Material.

3.2 Structural Framework

Facies transitions in the foreland basin resulted in a complex mechanical stratigraphy. This complexity was important for the structural style of the Subalpine Molasse, when ongoing progradation of the Alpine wedge resulted in inclusion of the proximal parts of the basin into the orogenic wedge (e.g., *Ganss and Schmidt-Thomé*, 1955; *Ortner et al.*, 2015) (see *Ortner et al.*, 2023, for a recent review). Complex structures make the interpretation of the subsurface challenging, and it has been shown that despite the extensive data set, different interpretations of the structures in the Subalpine Molasse are possible (*von Hagke and Malz*, 2018). Thrusting in the Subalpine Molasse commenced shortly after deposition of the sediments (*Burkhard and Sommaruga*, 1998; *von Hagke et al.*, 2012) and continued until late Miocene times, including reactivation of structures, as shown by thermochronolgical data and section balancing (*Mock et al.*, 2020; *von Hagke et al.*, 2012, 2014; *Ortner et al.*, 2015).

The thrusts that juxtapose the Northern

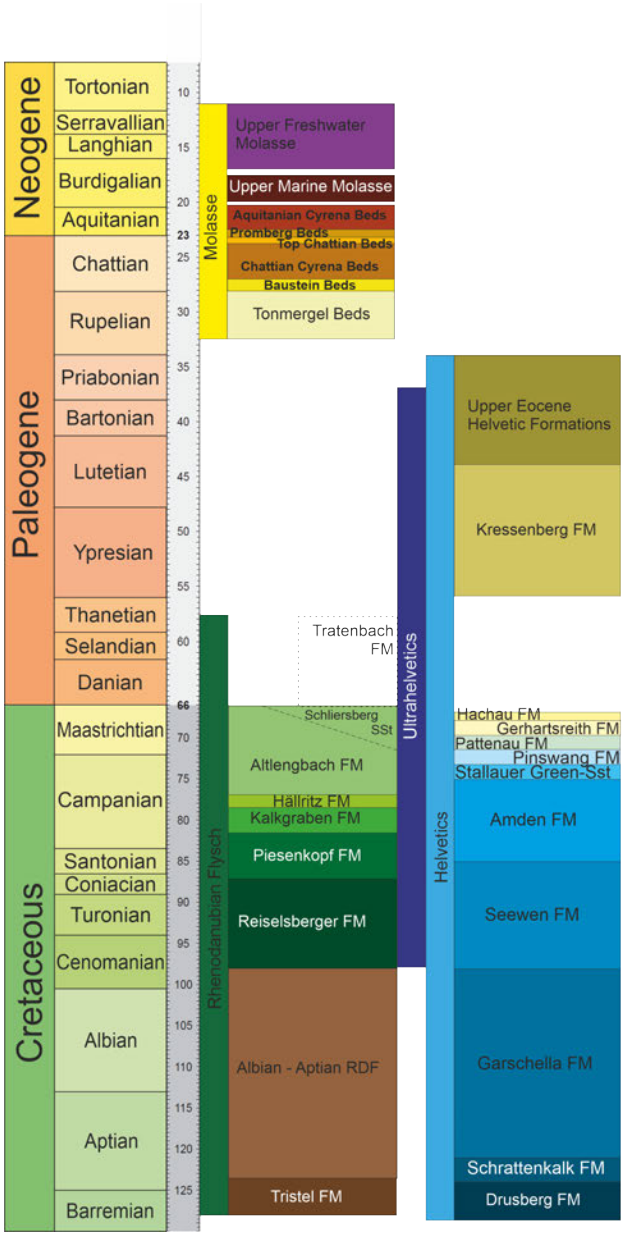

Figure 2 – Synthesized stratigraphic columns for the Rhenodanubian Flysch, Helvetic and Molasse units, compiled on basis of *Ostheimer and Schröder* (2016), *Pflaumann and Stephan* (1968), *Stephan and Hesse* (1966), *Paulus* (1963), *Ganss and Schmidt-Thomé* (1953), and *Stg* (2016). A detailed description of the stratigraphy can be found in the Supporting Information.

Calcareous Alps against the Rhenodanubian Flysch mark the southern boundary of the study area. Structures in the Subalpine Molasse between Bad Tölz and the river Inn can be subdivided into three tectonic slices, which we name MOL1-3 from south to north. (Figure 1). The southernmost slice (MOL1), immediately north of the basal thrust of the Rhenodanubian Flysch, includes the Hausham Syncline. The Mühlau and Leitzach Thrusts form the northern boundary of MOL1. Both faults and the Hausham Syncline are not mapped west of Bad Tölz, with an unclear structural termination possibly against a strike-slip fault zone (Ostheimer and Schröder, 2016). To the east, both faults merge

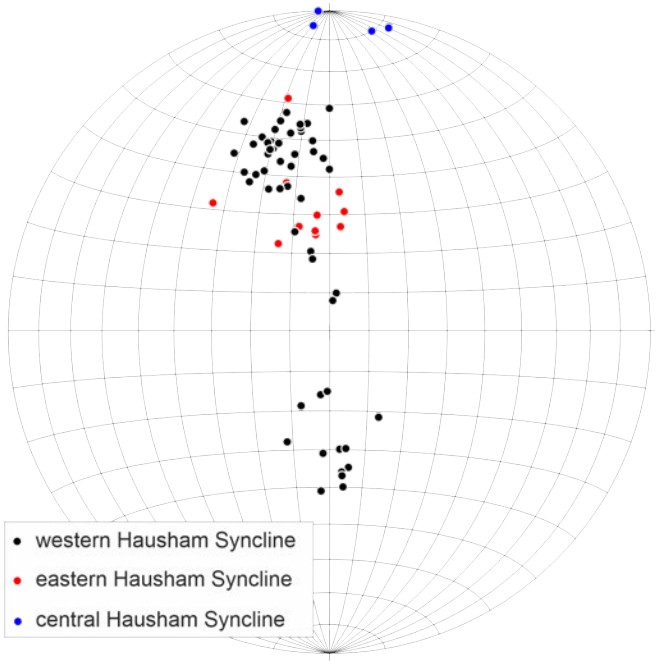

Figure 3 – Stereonet plot of new orientation data from the Hausham Syncline. Clusters show two fold limbs of medium dip angles in the western part (black), two parallel fold limbs dipping to the south in the eastern part (red) and steep dips of the southern limb in the central part of the syncline.

into the basal thrust of the Rhenodanubian Flysch, alongside with tapering out of the Hausham Syncline. The Hausham Syncline is an open fold in the west, but its southern limb is successively overturned towards the east (Figure 1, *Ortner et al.*, 2015; *Ganss and Schmidt-Thomé*, 1953). Bedding orientations measured at the surface in the Hausham Syncline area of the Subalpine Molasse show two clusters that represent the northern and southern limbs of the syncline (Figure 3). The change of the dip of the southern limb can be traced by separating the values geographically to a western and an eastern subset, with a boundary region between Lake Tegernsee and Lake Schliersee (Figure 1).

Slice MOL2, includes the Miesbach Syncline (*Ganss and Schmidt-Thomé*, 1953; *Ortner et al.*, 2015), while slice MOL3 represents all structures north of the Ellbach Thrust (Figure 1). West of the study area the leading edge of deformation of the Subalpine Molasse is a triangle zone, which develops into hinterland dipping thrusts of the Kirchbichl Thrust system in the eastern part of the study area (e.g., *Ortner et al.*, 2015; *Shipilin et al.*, 2020). The termination of the triangle zone within the study area is however poorly constrained. This, together with the poorly constrained strike-slip faults provides the main structural uncertainty of the study area. However, the large existing structural and stratigraphic data set allows to test modeling approaches as the influence of conceptual biases is decreased and models are much more data driven.

4 Geological Data and Modeling Approaches

We first describe the available geological data and then briefly present the geometric (steady state) and kinematic modeling approaches that we use in this work.

4.1 Geological Data

The 3-D structural model is built based on geological maps, seismic data, as well as borehole data. In addition, we conducted our own field work in order to reproduce published data and to complement missing information (see Supporting Information and data at https://doi.org/10.18154/RWTH-2023-08505). One focus of the field work was to obtain quantitative measurements of orientations where published data only provided qualitative indications. In addition, the aim was to obtain more detailed insight from local mapping in areas where the existing adjacent maps or cross-sections showed different interpretations. Overall, we further improved data density in regions where only little data are reported. We collected structural data points from previous studies (*Stephan and Hesse*, 1966; *Pflaumann and Stephan*, 1968; *Ostheimer and Schröder*, 2016) using georeferenced files of the associated maps and reading the position of the data points, as well as dip and dip direction from the indicators provided on the geological maps. We additionally digitized traces of layer boundaries. To obtain a 3-D dataset, we projected 2-D data onto the surface of a digital elevation model of the region based on SRTM data with a resolution of 90 m (*Jarvis et al.*, 2008).

In addition to the surface measurements and observations, we compiled the data of 112 shallow wells in the model (Bayrisches Landesamt für Umwelt, www.lfu.bayern.de). Most of these wells remain within the upper 100 m of the stratigraphic pile, and 18 wells include layer boundaries or faults. Our database furthermore includes stratigraphic logs of deep wells drilled in the region (*Paulus*, 1963; *Müller*, 1975; *Schmidt-Thomé*, 1949), as well as reprocessed seismic images close to the trace of the TRANSALP profile, covering the Subalpine Molasse of the study area (*Thomas et al.*, 2006).

Both modeling approaches are based on the same underlying data set and hence the overall quality of both models hinges on the quality of the input data. A typical error source in geological models is stratigraphic uncertainty, and particularly the thicknesses within the stratigraphic pile. By choosing the Subalpine Molasse, and our study are in particular, we are able to minimize this error. Stratigraphy of the Molasse has been extensively studied, and thickness variations are well known. For an extensive description of how we synthesized the wealth of stratigraphic data into one consistent column, the reader is referred to the Supplementary Material. Additional potential error sources are quality of mapping and accuracy of dip indicators on the maps, the quality of georeferencing, the DEM used, and the error in reading the orientation of the dip indicators, as well as uncertainties of well logs. The effect of these errors depends on the scale of the models. For our kilometer-scale models, errors of datapoint-positioning based on the existing high resolution topographic data are small and should fall in the range of few meters or tens of meters. Errors in dip and dip azimuth measurements vary with the quality of the measured surface. These errors can be as small as 1° (reading precision of compass) but increase for small or uneven surfaces and possibly tilted outcrops by erosion or vegetation cover. Some mapping studies partly provide only qualitative dip values differentiating between vertical, steep, medium, shallow, and horizontal dips (e.g., *Ostheimer and Schröder*, 2016; *Pflaumann and Stephan*, 1968; *Stephan and Hesse*, 1966). Where we could not re-map the structures, this data introduces uncertainty into the model.

4.2 Modeling Workflow

For modeling, we focus on the Subalpine Molasse as the main scope of this study. Data compiled for the Helvetic and Rhenodanubian Thrust sheets feed into the discussion of modeled structures. In the following, we first describe the modeling approaches separately, before discussing their individual strengths and weaknesses, and how they could possibly be combined.

4.2.1 Cross-section Interpretation and Balancing

We use MOVE (*Petex*, 2018) to build cross-sections based on structural interpretation that is consistent with the available data. To minimize boundary effects in the model, we included data from outside the study area. This comprises well data and surface data that are located up to 10 kilometers outside of the study area.

For cross-section balancing, we created five N-S trending sections, i.e., oriented approximately perpendicular to the general strike of structures. We located these sections at the ends of the Hausham Syncline, and three in the area where the southern limb of the syncline progressively overturns from northward dipping in the west to southward dipping in the east (Figures 1 and 3). We projected structural data within one kilometer distance into the cross-sections, data of deep wells within five kilometers, collected intersections of layer boundaries and faults with the section planes, and projected the seismic images of *Thomas et al.* (2006) (trace in Figure 1) onto the neighboring three central cross-sections.

For kinematic restoration of the sections, we focused on the central part of the study area including the Hausham Syncline and used the three cross-sections that cover this structure (2–4). For

the westernmost cross-section (1), we obtained two different structural interpretations and subsequently balanced both. One includes the continuation of the frontal triangle zone that is reported further west and one with hinterland dipping thrust only, as reported further east (e.g., *Berge and Veal*, 2005; *Ortner et al.*, 2015).

Cross-section balancing is based on the principle that post-depositional concentric deformation processes do not produce changes in rock volume and thus, bed-length in a cross-section must remain constant (*Dahlstrom*, 1969). This assumption may be problematic in cases where in addition to faulting, strain is accommodated within the stratigraphic pile as distributed deformation such as pressure solution or small-scale faulting (e.g., *Groshong*, 1975; *Wojtal*, 1989). Such distributed deformation (or penetrative strain) may be as small as 2%, but can reach up to 30% of total shortening (see e.g., *Burberry*, 2015, for a review). In the Subalpine Molasse a limited amount of pressure solution features exists and, generally, the amount of penetrative strain seems to be small. This is expected, as the sequence is dominated by siliciclastic rocks that probably have not been substantially heated after deposition as indicated by thermochronological data in adjacent regions (*von Hagke et al.*, 2014). We therefore do not include an estimation of shortening associated with distributed deformation into our models.

In kinematic restorations, geometric validity of cross-section interpretations can be tested by measuring the lengths of beds between vertical reference lines in positions where layer-parallel slip can be ruled out (*Dahlstrom*, 1969). As the kinematic restoration tools of MOVE software cannot balance overturned structures, we improved restorations by hand using line-length balancing on the basis of *Dahlstrom* (1969). We measured the lengths of beds between the reference position or faults on the interpreted cross-sections and drew straight lines of the according lengths at distances resembling bed thickness, starting at the reference line. When a bed terminates at a fault, this fault is marked in the balanced section and serves as a new reference line for the next line segment.

Another assumption in cross-section balancing is a foreland-propagating thrust sequence (*Boyer and Elliott*, 1982). This assumption is important to prevent truncation of structures in thrust systems dominated by ramp-flat-structures, which would hinder balancing. In the thrust system described here, *von Hagke et al.* (2014) and *Ortner et al.* (2015) recognized a hinterland-breaking thrust sequence, in which thrusting was preceded by folding. In foreland-propagating thrust systems, line-length balancing will result in a hinterland-dipping attitude of future ramps. However, in hinterland-breaking thrust systems, faults will cut across already deformed and folded beds. Line-length balancing of such thrust systems will result in excess line length where folds are cut, and thus foreland-dipping segments of thrust faults.

4.2.2 Geometric Steady-State Modeling with GemPy

The aim of surface-based geometric modeling is to obtain representations of relevant geological features in 3-D space (e.g., *Wellmann and Caumon*, 2018). To interpolate between, and to extrapolate beyond, the available geological data (Section 4.1), we employ here a global co-kriging interpolation approach (*Lajaunie et al.*, 1997), implemented in the open-source software GemPy (*de la Varga et al.*, 2019). Surface positions are treated as isopotentials in a global scalar field in an implicit representation. The field values themselves are obtained through a co-kriging of surface contact points and orientation measurements. This combination enables the direct consideration of orientation measurements at any point in space in the interpolation step. This is an advantage when considering the typical field observations that we use in our case, as contacts between geological layers are often not outcropping, whereas orientation measurements can be taken at many locations in the area. Age relationships are defined in the continuation of the scalar field in space, and multiple sequences, separated by faults or unconformities, can be modeled through an interaction of multiple scalar fields. For more details on the method, see *de la Varga et al.* (2019), *Brisson et al.* (2023) and the online website of GemPy (www.gempy.org).

In the current version, GemPy faults are modeled as infinite surfaces. The Ellbach Thrust is therefore not modelled as it terminates eastwards within the model volume. The same applies for the northernmost fault strand of the Kirchbichl Thrust that is present in the eastern part but terminates to the west. Also, this causes limitations to uncertainty modeling of fault systems, as discussed later.

4.2.3 Probabilistic Modeling with GemPy

In addition to steady-state geometric modeling, GemPy also enables a probabilistic geological modeling approach as a way to evaluate model uncertainties due to uncertain input data (e.g., *Wellmann et al.*, 2010). In order to perform probabilistic geomodeling, information about the statistical distribution of input parameters is required.

As uncertainty modeling of fault systems is limited (see above and discussed below), we focused on the Hausham Syncline in the part where it overturns in a first probabilistic model. To reduce computational time, prior to analysis we removed redundant data points that contain the same information as adjacent data, such as identical dip/dip azimuth values. Uncertainty analysis in GemPy is done by assigning stochastic (normal) distributions to the data points instead of the fixed locations

used for the geometric models (*de la Varga et al.*, 2019). Consequently, integration of measurement and interpretational errors associated with the data points into the modeling process is possible. Such errors include GPS uncertainty, errors of maps and reading coordinates from maps, errors of elevation models and of structural measurements. Other error sources such as associated with penetrative strain or stratigraphic thickness have not been included in the uncertainty estimates (see above).

With these normally distributed data points, we conducted a Monte Carlo type simulation. A thousand models were computed, with one value drawn out of the normal distribution for each data point in each model run. As model output, each model voxel is assigned to a certain lithology in each model run, depending on the placing of the boundaries. The thousand model outcomes provide stochastic distributions of the different lithologies for each voxel. Concerning all voxels within the 3-D model volume, the result is a probability field displaying placing of boundaries and thus geologic layer assignment stochastically.

From the 3-D probabilistic model, we computed four cross-sections, one containing the western open part of the Hausham Syncline, one including the steep southern limb in the central part, and one the overturned limb in the eastern part. The fourth is covering the syncline along-strike. Using the DEM, we additionally computed a probabilistic geological map. The cross-sections and the map show the probability fields of all the stratigraphic formations, as well as the Sharmon cell entropy of the model. This can be understood as a summary measure combining the probability fields for multiple stratigraphic formations in a single representation of uncertainty (*Wellmann and Regenauer-Lieb*, 2012).

5 Results

5.1 Geometric Modeling with MOVE

Within the tectonic slice MOL1, the southern limb of the Hausham Syncline is successively overturned from west to east (Figures 5a, 6a, and 7a). In the overturned part, the basal thrust of the Helvetic units is parallel to bedding of the southern limb of the Hausham Syncline (Figure 7a). The Mühlau Thrust forms the boundary between the slices MOL1 and MOL2. The distance between the Mühlau and Leitzach Thrusts ranges between 250 m and 1000 m at the surface, while both faults are consistently interpreted as strands of the same thrust at depth (Figures 5a, 6a, and 7a). In the easternmost section (5), the Leitzach Thrust includes a splay fault (Figure 8). Mühlau and Leitzach Thrust are not present in cross-section (1), as well as the whole slice MOL1 (Figure 4a-b). Data density and resolution of the stratigraphic differentiation do not allow for a precise interpretation of the internal structure of slice MOL2. Our models suggest it is dominated by an overturned syncline in the south that is cut by the Leitzach Thrust along the hinge zone. In section (2) (Figure 5a) the thrusted part of the syncline is narrower than further east. We interpret the northern part of slice MOL2 to feature a rollover anticline where the bounding thrust system flattens. The Ellbach Thrust and the Kirchbichl Thrust bound the tectonic slice MOL 3. The thrusts have variable distances, ranging from approximately 1500 m in cross-section (1) (Figure 5a-b) to approximately 400 m in cross-section (3) (Figure 6a). It is difficult to follow the Ellbach Thrust to the east. We cannot determine whether it ceases eastwards between section (1) (Figure 4a-b) and section (2) (Figure 5a) and forms a relay with the southernmost thrust of the Kirchbichl Thrust splays, or if it continues and forms the southernmost strand of that system in the east. The internal architecture of the frontal thrust zone (Kirchbichl Thrust) does not substantially change along-strike in the central and eastern part of the study area, being four strands emerging from a flat basal thrust on top of the Promberg Beds. The northernmost strand is dipping towards the west and thus a blind thrust in section (3) and not present in section (2) (Figures 5a, 6a, and 7a). Bedding within the slices is steep to overturned. Only the westernmost section (1) is interpreted differently (Figure 4a-b), where surface and borehole data allow different interpretations: only one major internal slice instead of two or three (Figure 4a), as proposed by *Paulus* (1981, their Figure 4a), or the presence of a triangle zone ceasing to the east (Figure 4b). This triangle zone has been documented farther west (e.g., *Ortner et al.*, 2015; *Shipilin et al.*, 2020). Even though the interpretation of this small triangle zone is in accordance with most of the data compiled by us and used by *Paulus* (1981) to infer hinterland dipping thrusts, stratigraphic and structural data from the Koenigsdorf-1 well (*Paulus*, 1963) shows no indication of a backthrust.

5.2 Kinematic Modeling

In the balanced cross-sections, features exist that result from the break-back sequence of thrusting. Particularly the “floating” of the most frontal thrust imbricate in the reconstruction (Figure 4c) as well as the overturned faults (Figures 5c, 6c, 7c) are a result of the break-back sequence. Total shortening within the Subalpine Molasse is estimated to be 3500 m for cross-section (1) (Figure 4c-d), 5600 m along cross-section (2) (Figure 5c), 6700 m in cross-section (3) (Figure 6c) and 6300 m for cross-section (4) (Figure 7c). This marks an increase in overall shortening from west to east. Comparing the different cross-sections, the total amount of shortening is additionally distributed unevenly between the individual tectonic slices (MOL1-3). Table 1 summarizes the quantified thrust movements and shortening results for the four balanced cross-sections. In the following, we present the restoration results slice by slice along the strike

Table 1 – Balancing results for cross-sections (1) to (4) (Figures 4c, 5c, 6c, and 7c). Overall shortening is original length of the Baustein Beds minus recent horizontal distance between two reference locations (line length method). Shortening by folding is the line length result for single synclines. Fault movements (offset) are distances of equal horizons along a thrust. For Mühlau thrust, Fault movement is calculated using the overall thrusting of the Mühlau-Leitzach system minus the value for the Leitzach Thrust.

		Shortening by folding			Movement on faults								
Section	Overall shortening (BS Base, m)	Hausham Syncline (BS Top, m)	Miesbach Syncline (BS Top, m)	Kirchbichl Syncline (BS Top, m)	Mühlau (m)	Leitzach (m)	Ellbach (m)	KB system (m)	KB prox. (m)	KB middle (m)	KB frontal (m)	KB north (m)	Triangle structure (m)
1 (triangle)	3500		600	150			70	2400	2300				100
1 (HDT)	3500		600	150			70	2400	1400	1000			
2	5600	650	1300		290	350		4600	2170	230	2200		
3	6700	1200	1100		1230	100		5000	3050	450	1500	0	
4	6300	1500	1300		560	100		4900	2920	160	1600	220	

of structures, starting at the deformation front with slice MOL3. For the westernmost cross-section (1) (Figure 4c-d) we obtain 70 m of offset on the Ellbach Thrust. For the Kirchbichl Thrust we obtain an offset of 2400 m of shortening. Interpreting the structure as the termination of the triangle zone (Figure 4d), 100 m of this shortening occurred along the backthrust. For the splay-thrusts interpretation, 1000 m of shortening occurred along the frontal thrust and subsequently 1400 m in the southern branch (Figure 4c). 19 km farther east in cross-section (2) (Figure 5c), the triangle zone has pinched out, and consequently only the geometry with hinterland dipping thrusts needs to be regarded. Balancing results in 4600 meters of thrust movement on the Kirchbichl Thrust. This value is similar to cross-sections (3) and (4) further east (Figures 6c, 7c), where restoring the Kirchbichl Thrust and its splays yields shortening values of 5000 m for cross-section (3), and 4900 m for cross-section (4). Offsets of the individual thrust splays are listed in Table 1. In summary, the Kirchbichl Thrust shows comparable amounts of overall shortening from the central study area to the east, regardless of whether there are three or four fault strands. Distribution of shortening between the individual strands varies according to our geometric interpretation. In the westernmost part, where geometry changes, the shortening estimates drop to about half of the magnitude obtained further east. MOL3 in the westernmost section features the Kirchbichl Syncline, which takes up 150 m of shortening along cross-section (1).

In the Mühlau and Leitzach Thrust system (slice MOL2), kinematic restorations show large variability between the different cross-sections (Table 1). In cross-section (2) (Figure 5c), strain is distributed approximately equally between the two strands, with 290 m for the Mühlau Thrust and 350 m for the Leitzach Thrust. Five kilometers farther east in cross-section (3) (Figure 6c), balancing yields only 100 m of offset on the Leitzach Thrust but 1230 m on the Mühlau Thrust, thus a total of 1330 m of thrusting. For cross-section (4) (Figure 7c) total shortening decreases to 660 m, subdivided into 100 m shortening on the Leitzach Thrust and 600 m shortening on the Mühlau Thrust. We note that the interpretation of horizons to match across the Mühlau Thrust is uncertain due to the depth of the horizon in question (bottom of Tonmergel Beds), and the resulting distance to most data. Unfolding the Miesbach Syncline yields 600 m of shortening for cross-section (1) (Figure 4c-d), and similar values for the sections to the east with 1300 m for cross-section (2) (Figure 5c), 1100 m for cross-section (3) (Figure 6c), and 1300 m for cross-section (4) (Figure 7c). Concerning slice MOL1, shortening by folding of the Hausham Syncline yields 650 m for cross-section (2) (Figure 5c), 1200 m for cross-section (3) (Figure 6c), and 1500 m for cross-section (4) (Figure 7c). This marks increased shortening as the southern limb of the syncline successively overturns towards the east.

5.3 Geometric Modeling with GemPy

The geometric model of the entire Hausham Syncline shows that the southern limb of the syncline steepens from west to east and overturns near the eastern end (Figure 9). East of the overturned part, the structure opens again. The model also shows widening of the syncline where the amount of data points is low. Especially, where the southern limb is overturned, the lack of subsurface data leads the algorithm to interpolate a hose-like structure reaching to the bottom of the model (Figure 9a). We therefore chose to insert data points taken from the seismic interpretation made in MOVE, as the seismic line crosses that part of the syncline. Points added mostly represent the lower boundary of the Baustein Beds and constrain the shape of the syncline. The result with these added points is given in (Figure 9b).

Data points representing the locations of the thrusts bounding the Hausham Syncline are added to the database and, subsequently, the thrusts are modeled (Figure 9c). The basal thrust of the Helvetics is vertical in the west and shallows towards the east, where it is parallel to the overturned southern limb of the Hausham Syncline. The Mühlau and Leitzach Thrusts are two strands of the same thrust at depth.

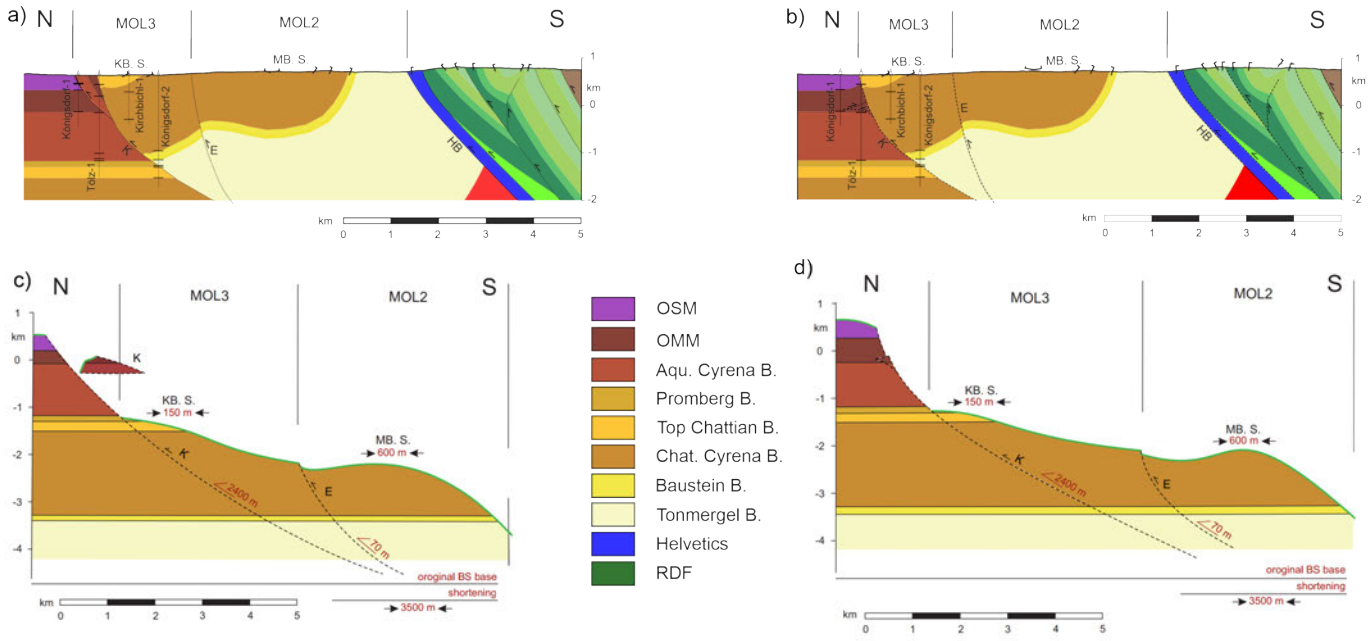

Figure 4 – Steady state geometric interpretation and kinematic restoration of cross-section (1) (Figure 1). **a)** Interpretation of a hinterland dipping thrust. **b)** interpretation of a small triangle zone, **c)** kinematic restoration of a), **d)** kinematic restoration of b). Kinematic restorations comprise quantifications of shortening by folding and offset of thrusts, as well as overall shortening determined by the line length method (see Table 1). RDF (green colors): exemplarily interpreted for this section, but beyond the scope of this study. MOL1-3: tectonic slices of Subalpine Molasse, KB. S.: Kirchbichl Syncline, MB. S.: Miesbach Syncline, K: Kirchbichl Thrust, E: Ellbach Thrust, HB: Helvetics Base Thrust. Wells Kirchbichl-1, Königsdorf-1 and Königsdorf-2 (*Paulus*, 1963) projected to the section.

They are subparallel to each other in the western and eastern part. In the central part from east of Bad Tölz to Lake Schliersee, the Mühlau Thrust is much steeper than the Leitzach Thrust. In this part, the slice between both thrusts widens.

While the previously introduced model focused on slice MOL1, we created a full stratigraphic plus structural model for the central part of the study area, including all slices of the Subalpine Molasse and the undeformed Molasse it overrides (Figure 10). The dataset comprises the structural raw data and datapoints taken from the interpreted cross-section (2-4) (Figures 5c, 6c, and 7c).

North of the deformation front, the 3-D model shows drag folding of the Molasse units, which is consistent with the steeply inclined strata mapped just north of the frontal thrust of the Kirchbichl Thrusts (Figure 10a). North of this structure, the undeformed Molasse appears flat lying with minor undulations that show increasing amplitude away from data points. Especially in the central-western part, the drag fold is more pronounced than elsewhere along-strike. In map view (Figure 10b), the surface traces of the Kirchbichl Thrusts bend southward, concordant with the position of the Taubenberg Fan (Figure 1). The layer boundary of the Upper Freshwater and Marine Molasse bends towards the north west and east of this bend. Internally, the Kirchbichl Thrust system (red thrusts) shows two slices of constant width. Strata within the slices of the Kirchbichl Thrust is steeply inclined to overturned (Figure 10c). Tectonic slice MOL2 (between the red Kirchbichl Thrust and the blue Mühlau and Leitzach Thrusts) exhibits drag folding on both bounding faults (Figure 10a-c). In the north the slice resembles the hanging wall of the Kirchbichl Thrust. Here data of a mapped narrow anticline result in the interpolation of the drag fold in the models. At the southern rim, where slice MOL2 is the footwall of the Leitzach Thrust, overturned orientation values result in modeling of a pronounced drag fold along this structure. The central part of slice MOL2 is dominated by a syncline bridging between both rim structures. This syncline resembles the Miesbach Syncline mapped in that area (Figure 1). Away from data points, the model tends to show straight and northwards tilted strata instead of the folding pattern (Figure 10a-c). The thin slice between the Leitzach and Mühlau Thrusts even narrows in the central part of the model and widens towards the east (Figure 7a, b, c), which is consistent with maps of the area (*Pflaumann and Stephan*, 1968; *Stephan and Hesse*, 1966). The model shows a strong southward excursion of the Leitzach Thrust to the west, which is the reason for the narrowing of the slice. The Mühlau Thrust follows this course to the west, while it bends southward away from the Leitzach Thrust in the east. The strata within this slice dips steeply or is overturned, parallel to the drag fold in the footwall of the Leitzach Thrust. Tectonic slice MOL1 includes the Hausham Syncline. The northern limb exhibits constant southward dipping beds, while the southern limb is dipping towards the north at the western rim but successively overturns towards the east. Along the northern rim of the

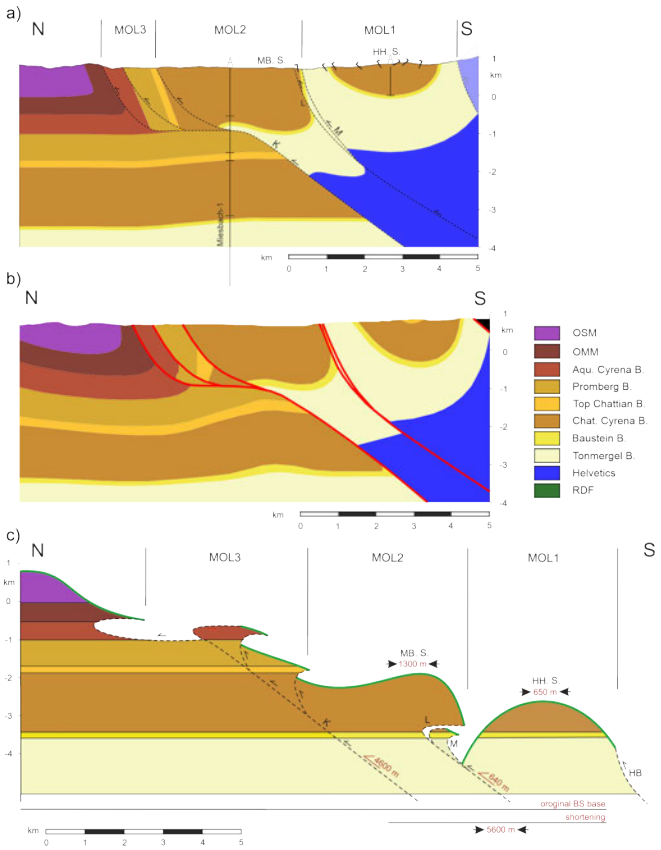

Figure 5 – Cross-section (2) (see location in Figure 1). **a)** Steady state geometric interpretation. Light shaded area is not modeled with GemPy. **b)** Cross-section computed from GemPy 3-D model, black area is not modeled, **c)** kinematic restoration, comprising quantifications of shortening by folding and offset of thrusts, as well as overall shortening determined by the line length method (see Table 1). MOL1-3: tectonic slices of Subalpine Molasse, MB. S.: Miesbach Syncline, HH. S.: Hausham Syncline, K: Kirchbichl Thrust, L: Leitzach Thrust, M: Mühlau Thrust, HB: Helvetics Base Thrust. Miesbach-1 well (*Müller*, 1975; *Risch*, 1993), and well in MOL1 (Bayrisches Landesamt für Umwelt, www.lfu.bayern.de) projected to the section.

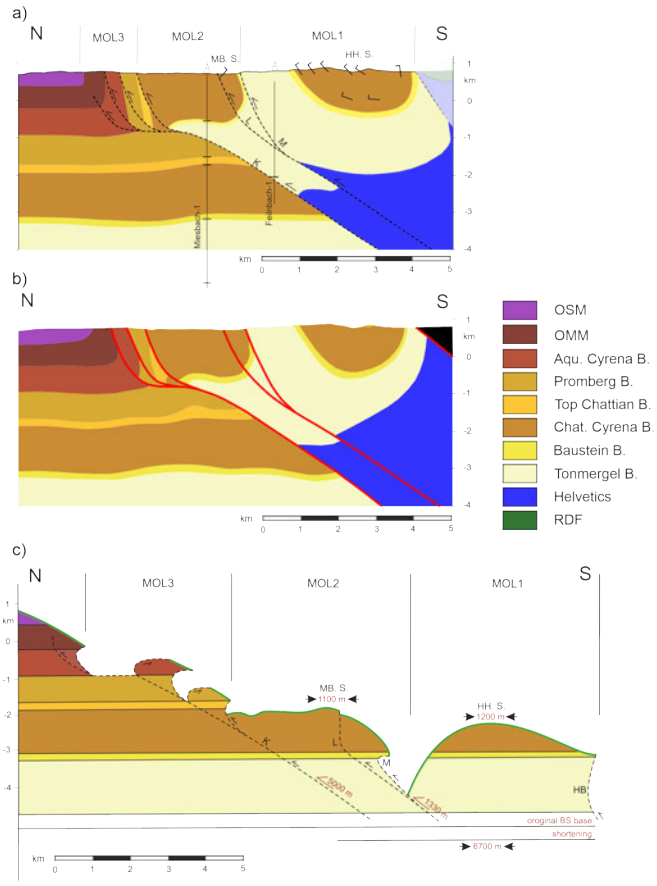

Figure 6 – Cross-section (3) (see location in Figure 1). **a)** Steady state geometric interpretation. Light shaded area is not modeled with GemPy. **b)** Cross-section computed from GemPy 3-D model, black area is not modeled, **c)** kinematic restoration, comprising quantifications of shortening by folding and offset of thrusts, as well as overall shortening determined by the line length method (see Table 1). MOL1-3: tectonic slices of Subalpine Molasse, MB. S.: Miesbach Syncline, HH. S.: Hausham Syncline, K: Kirchbichl Thrust, L: Leitzach Thrust, M: Mühlau Thrust, HB: Helvetics Base Thrust. Miesbach-1 well (*Müller*, 1975; *Risch*, 1993), and Feilnbach-1 well (*Paulus*, 1963) projected to the section.

slice the model includes a drag anticline attached to the Mühlau Thrust. In the center of the Hausham Syncline the model predicts the presence of Top Chattian Formation in outcrop. The basal thrust of the Helvetic units overrides MOL1 in the south and marks the boundary of the model.

We computed cross-sections cutting N-S through the 3-D model created with GemPy (Figures 5b, 6b, and 7b). These are located approximately along the sections we constructed with MOVE. The 3-D model derived cross-sections show very similar geometries compared to the interpreted 2-D cross-sections. The northernmost splay of the Kirchbichl thrust cannot be modeled, as modeling finite faults is so far not included in GemPy. Obvious differences occur away from data points, where GemPy computes more wavy surfaces than interpreted (north of the thrusts). The depth of the synclines and thus their respective shapes differ as well. While the Gempy models prefer smooth dip changes along the fold limbs, the geometry of the solutions obtained with MOVE are characterized by narrower hinge zones more comparable to box folds. This difference is a result of the low data density at depth, and associated uncertainty. In a well-studied region like our study area, fold geometries are well known. In areas of unknown fold geometries, GemPy models can show the range of possible geometries, especially when applying probabilistic modeling.

5.4 Probabilistic Modeling with GemPy

We present a probabilistic model of the central part of the Hausham Syncline. Three profiles intersect the model where balanced profiles (2-4) are located (Figures 11 and 12a-b), while one is located parallel to the strike of the syncline in its center (Figure 11d). Additionally, we present a probabilistic map derived from the model (Figure 12c). The westernmost cross-section (P1) contains the open part of the Hausham Syncline (Figure 11a). The probability field of the Lower Bunte Molasse shows an approximately

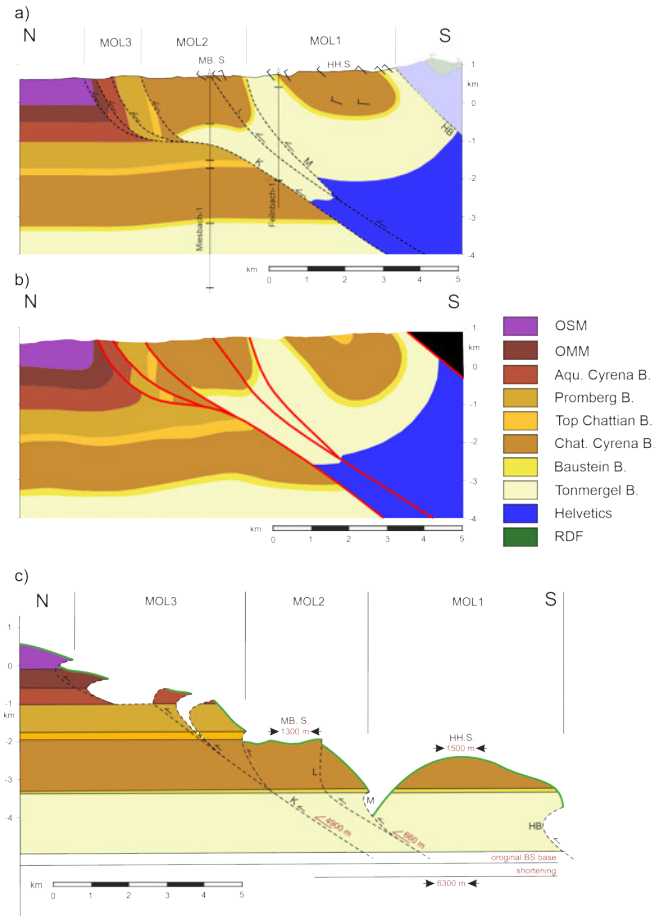

Figure 7 – Cross-section (4) (see location in Figure 1). **a)** Steady state geometric interpretation. Light shaded area is not modeled with GemPy. **b)** Cross-section computed from GemPy 3-D model, black area is not modeled, **c)** kinematic restoration, comprising quantifications of shortening by folding and offset of thrusts, as well as overall shortening determined by the line length method (see Table 1). MOL1-3: tectonic slices of Subalpine Molasse, MB. S.: Miesbach Syncline, HH. S.: Hausham Syncline, K: Kirchbichl Thrust, L: Leitzach Thrust, M: Mühlau Thrust, HB: Helvetics Base Thrust. Miesbach-1 well (*Müller*, 1975; *Risch*, 1993), and Feilnbach-1 well (*Paulus*, 1963) projected to the section.

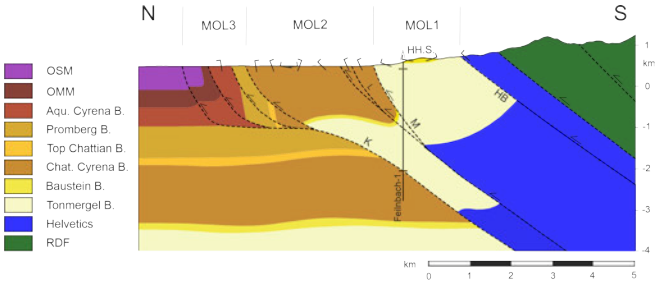

Figure 8 – Steady state geometric interpretation of cross-section (4) (see location in Figure 1). MOL1-3: tectonic slices of Subalpine Molasse, HH. S.: Hausham Syncline, K: Kirchbichl Thrust, L: Leitzach Thrust, M: Mühlau Thrust, HB: Helvetics Base Thrust. Feilnbach-1 well *Paulus* (1963) projected to the section.

200 m wide zone where the probability of finding the lithology decreases from 100% to 0%. This means that the Lower Bunte Molasse beds have to fall within this 200 m wide region, and models mapping the Lower Bunte Molasse elsewhere are geologically not viable. This zone does not widen away from the data points at the surface. This is reflected by the increasing probability of the Lower Chattian Coal FM at the boundary to the Lower Bunte Molasse. The lower boundary to the Baustein Beds exhibits a wider zone of medium probabilities on the northern limb of the syncline (Figure 11). In this part, the Baustein Beds show two clusters of elevated probabilities, with higher probability values for the cluster at lower depth. The maximum probability of 100% is not reached for the Baustein Beds. This is partly because of the separation into two possible depth intervals, and partly due to the low thickness of the formation. Shannon cell entropy plots (Figures. 11, 12) can be used to identify areas of higher or lower uncertainty and can be seen as an overall measure of misfit (*Wellmann and Regenauer-Lieb*, 2012; *Brisson et al.*, 2023). The entropy of the cross-section yields medium values for the boundary region between the Lower Bunte Molasse and Lower Chattian Coal FM and high entropy where the thin Baustein Beds and the Lower Chattian Coal FM are expected, as well as the underlying Tonmergel Beds (Figure 11).

Cross-section (P2) includes the steep southern limb of the Hausham Syncline (Figure 11b). The northern limb exhibits narrow zones where probabilities for all three formations drop from high values (close to 100%) to 0%. This is because two data points are located close to the section trace. The southern limb is constrained by a data point of the Baustein Beds, causing a similar sharp drop in probabilities at the Baustein Beds – Tonmergel Beds boundary. The layer boundary of the Lower Bunte Molasse and the Lower Chattian Coal FM is less certain, with an approximately 100 m wide zone where both formations are possible (Figure 11b). The clustering of the Baustein Beds on the northern limb, comparably to the observation in cross-section (P1) (Figure 11a), is also present in cross-section (P2) (Figure 11b). With increasing depth, the probability fields divert from the shape of a parallel fold. The entropy field, as well as the probability field of the Baustein Beds and Lower Chattian Coal FM, reveal that many model runs do not connect both limbs at all, resulting in continuation of the formation at depth towards the south.

The overturned southern limb is covered by cross-section (P3) (Figure 11c). Close to the surface, all layer boundaries show narrow zones where probabilities drop from high values to 0%. On the southern limb the lower boundary of the Lower Chattian Coal FM dips less steeply than the upper boundary. The reason is that the upper boundary is dominated by orientation data farther west, where the limb is steeper. At depth on the northern limb an additional data point reduces the entropy and consequently increases layer probabilities. At the hinge zone, the entropy is high where the probability fields of Lower Chattian Coal FM, Baustein Beds and Tonmergel Beds overlap. The entropy field shows

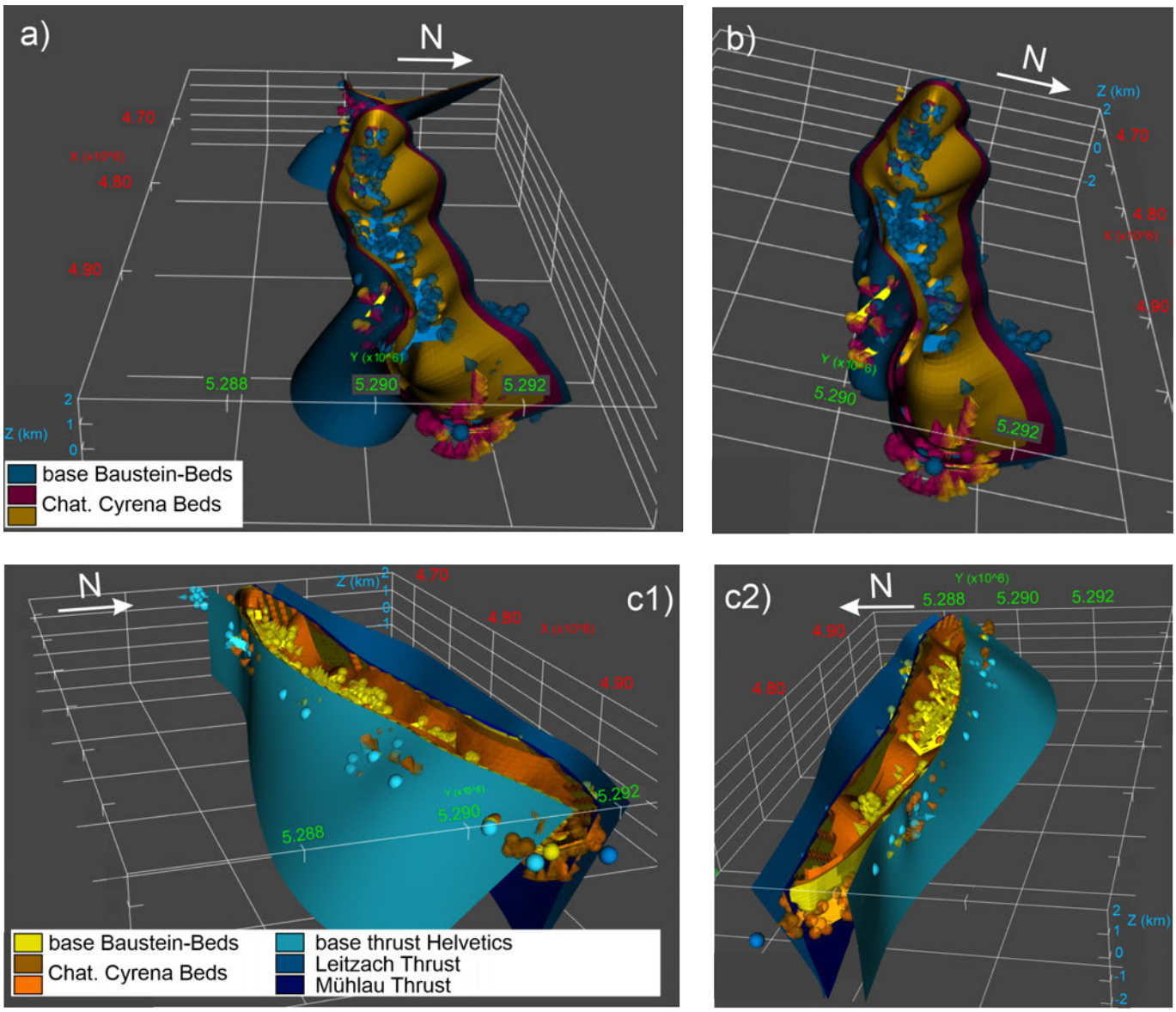

Figure 9 – GemPy 3-D models of the Hausham Syncline. **a)** Using points from own field work, existing maps (*Ostheimer and Schröder*, 2016; *Pflaumann and Stephan*, 1968; *Stephan and Hesse*, 1966) and wells (*Paulus*, 1963; *Müller*, 1975; *Risch*, 1993) only. **b)** Data points added from seismic interpretation, defining the subsurface location of the layer boundary between Baustein Beds and Tonmergel Beds of the Hausham Syncline. **c)** Model including the thrust bounding the Hausham Syncline (Helvetics Base Thrusts, Mühlau and Leitzach Thrusts). Horizontal scale: values along x and y axes multiplied by 10^6 refer to Gauss-Krueger Zone 4 coordinates.

that some of the models do not close the syncline and result in geologically meaningless open structures at depth, as for instance observed in cross-section (P2) (Figure 11b).

Cross-section (P4) transects the Hausham Syncline along-strike (Figure 11d). It shows that there are two depth-clusters of comparable modeled probabilities of the Lower Bunte Molasse – Lower Chattian Coal FM boundary in the western part. Subsequently, the Lower Chattian Coal FM and Baustein Beds exhibit two clusters, the shallower of which shows slightly higher probabilities. In the east a data point at depth resolves the clustering and the layer boundaries show low uncertainties. At the eastern end, pinching out of the Lower Bunte Molasse and replacing by Lower Chattian Coal FM is modeled by many of the model runs. It has to be noted that this is mostly above topography.

These uncertainties at depth are partly also reflected at surface. The probabilistic geological map shows that two different geometric interpretations are possible based on the input data. Either a narrow syncline exists in the western part, which widens towards the east, or the structure is rather cylindrical (Figure 12c). Slightly higher probabilities are obtained for the more cylindrical models (see Lower Chattian Coal FM).

In sum, probabilistic models show quantitatively how much uncertainties increase away from datapoints, which has been known qualitatively. This is especially relevant towards depth. The Hausham Syncline shows highest uncertainties of the models where the layer boundaries are

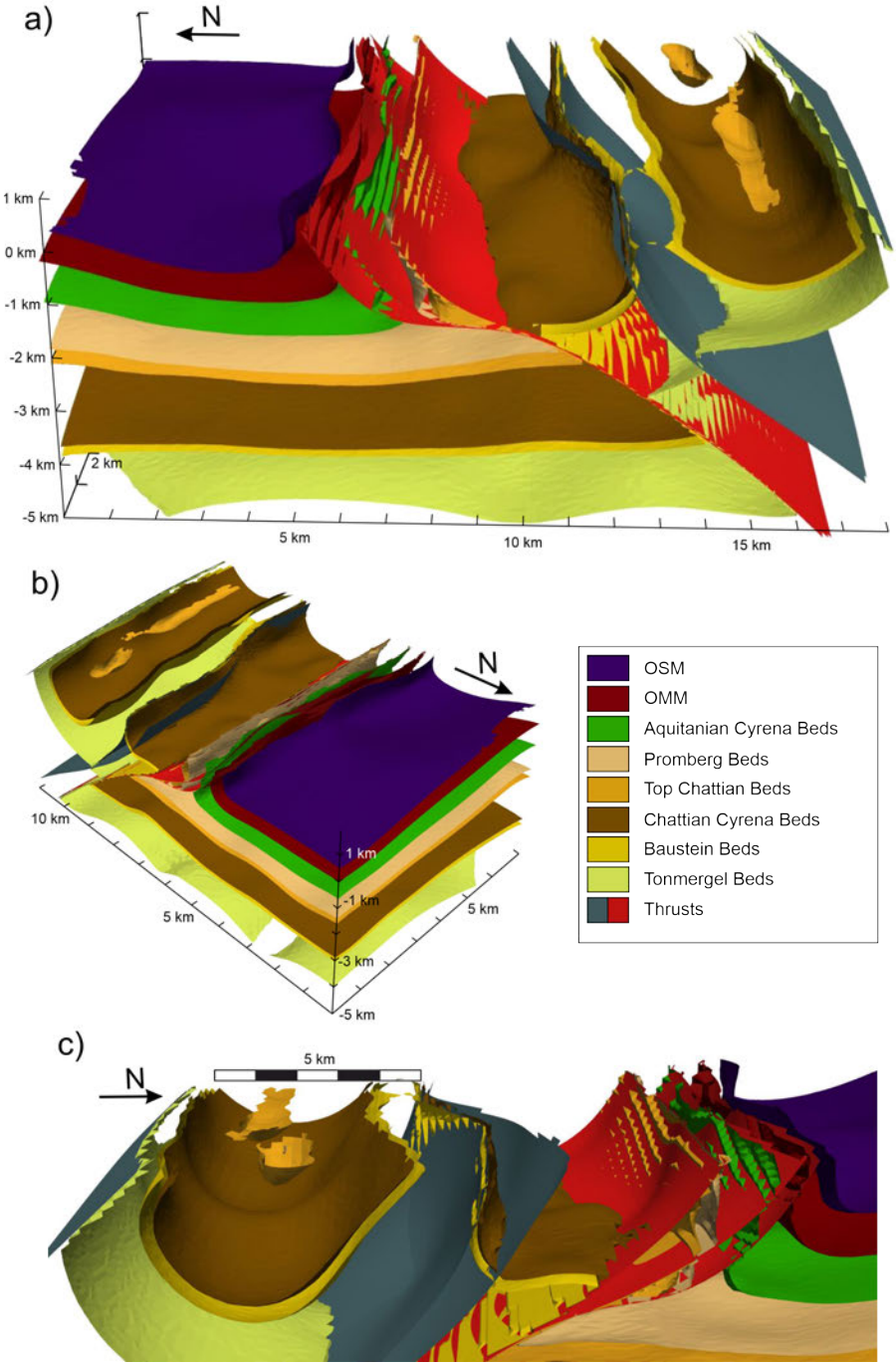

Figure 10 – 3-D model of the whole Subalpine Molasse between cross-section (2) and (4) (locations in Figure1). Data points are structural data from field work, existing maps (*Ostheimer and Schröder*, 2016; *Pflaumann and Stephan*, 1968; *Stephan and Hesse*, 1966) and wells (*Paulus*, 1963; *Müller*, 1975; *Risch*, 1993), as well as data points taken from the interpreted cross-sections (2) – (4). **a)** Complete model viewed from the top and W. **b)** Complete model viewed from the top and NE. **c)** Close-up of Hausham Syncline, Mühlau and Leitzach Thrust, as well as Kirchbichl Thrust viewed from the E.

overturned. GemPy modeling shows two competing versions of similar probabilities are possible: one of a narrowing syncline to the western part of the model, and a more cylindrical syncline.

6 Discussion

6.1 Constraints on the Geological Evolution Provided by the Combined Method

In this study, we focus on the structures of the Subalpine Molasse, while data and interpretations of the Rhenodanubian Flysch and Helvetic Thrust

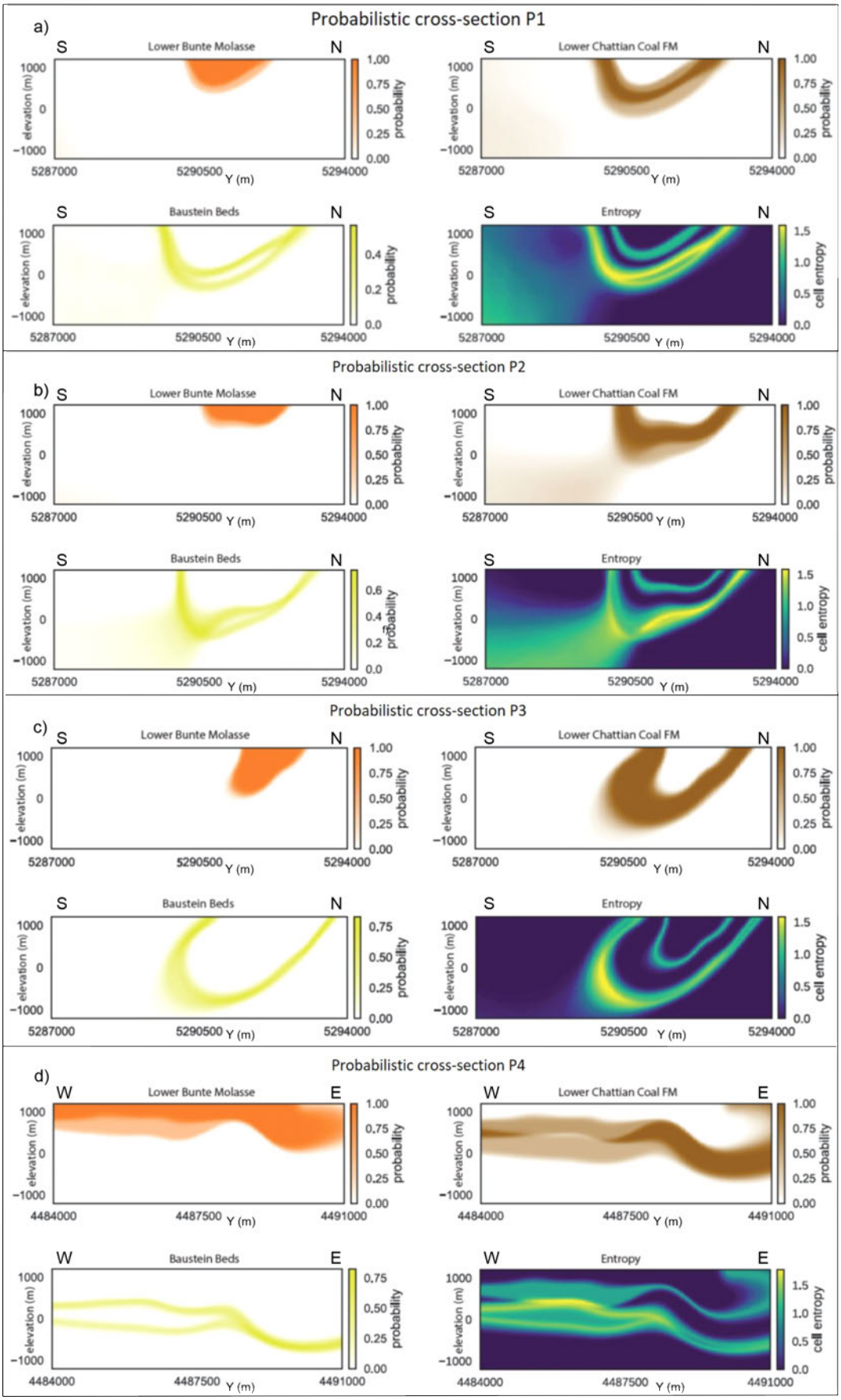

Figure 11 – Probabilistic models of the Hausham Syncline computed with GemPy. All probabilistic panels show the probabilities for Lower Bunte Molasse (orange), Chattian Cyrena Beds (brown) and Baustein Beds (yellow) to occur at the respective x-y coordinates. Entropy plots show high values where different units are obtained over 1000 model runs, with highest where all three units have equal probabilities. Locations of the sections are shown in Figure 12a. Y: Gauss-Krueger Zone 4 coordinates (N).

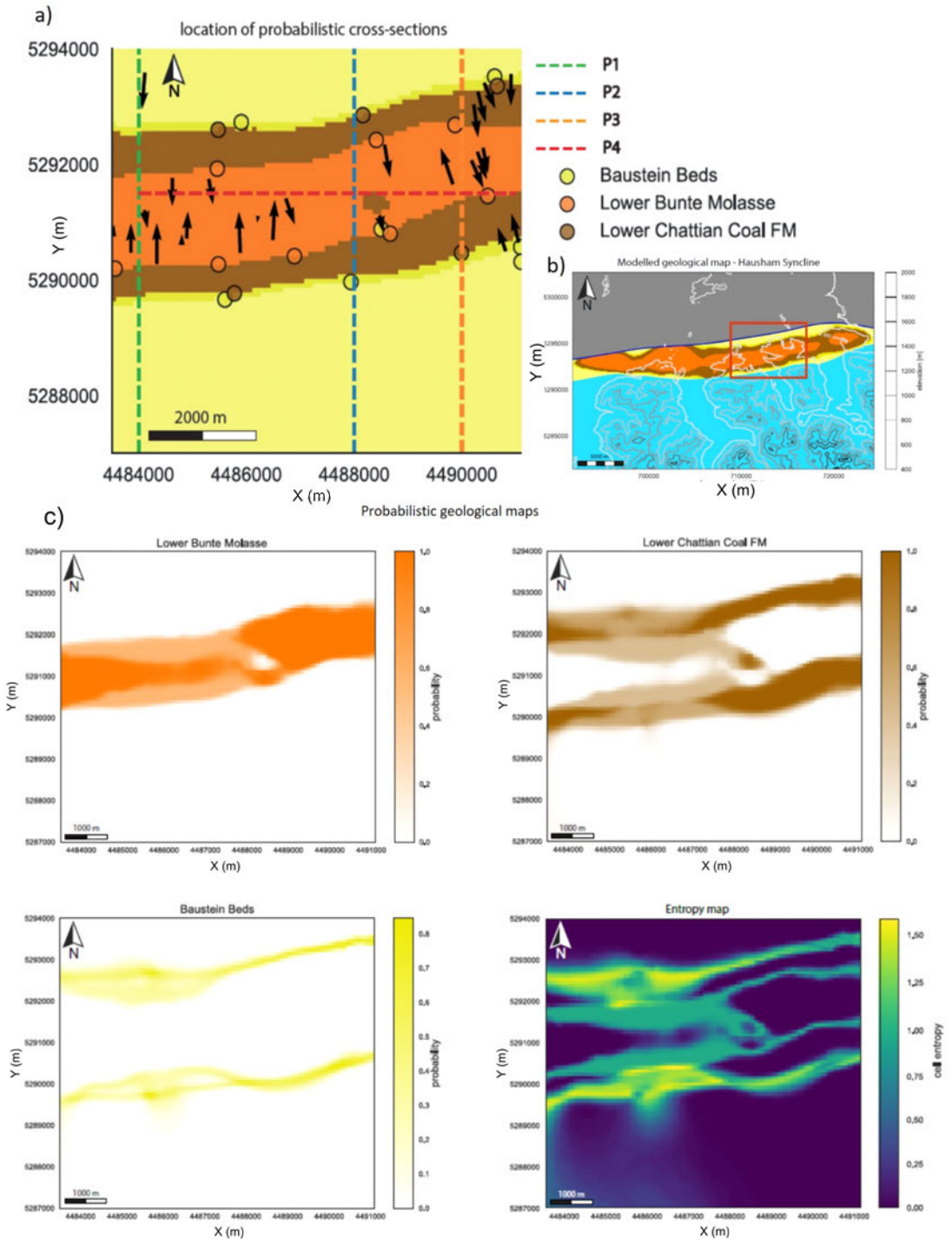

Figure 12 – Cross-section locations and probabilistics maps computed with GemPy. **a)** and **b)** show the location of the model volumes and the computed cross-sections of Figure 11. **c)** Probabilistic maps of the stratigraphic units modeled in the area in a). Scales in meters. X, Y: Gauss-Krueger Zone 4 coordinates (E, N), in b) UTM 32T coordinates.

Sheets are used to discuss potential links between the Subalpine Molasse and hinterland structures. A finer separation of the internal structures was not performed, as not considered to be relevant for the scope of this study. In the following, we discuss 3-D changes of geometries and kinematic differences along-strike, and compare our results to previous studies. In a first part, we discuss along-strike changes of the Hausham Syncline and the Kirchbichl Thrust. In a second part, we discuss strain distribution throughout the study area and compare our results to previous studies.

6.1.1 Along-Strike Geometries of the Hausham Syncline

The architecture of the Hausham Syncline is most easily interpreted as an open fold in the west with a gradual transition in the central part to an overturned southern limb in the east (Figures 4 to 11). Minimum shortening estimates of the Hausham Syncline resulted in 650 m in the open part (cross-section (2)) and 1500 m in the overturned part (cross-section (4)), with 1200 m in the transitional part (cross-section (3)) (Figures 5c, 6c, and 7c,

Table 1). Possible strike-slip faults along which the overturning is realized are not needed to explain the data. However, even though previous studies do not necessarily indicate such strike-slip faults within the Molasse (*Paulus*, 1963; *Ortner et al.*, 2015; *Ostheimer and Schröder*, 2016; *Pflaumann and Stephan*, 1968; *Stephan and Hesse*, 1966), based on the existing data set it is possible that such faults are present. NNE-SSW striking strike-slip faults have been mapped by previous studies in the Rhenodanubian Flysch thrust sheets (*Ostheimer and Schröder*, 2016; *Pflaumann and Stephan*, 1968; *Stephan and Hesse*, 1966) and in the Subalpine Molasse further west as well (Murnau Syncline, e.g., *Ortner et al.*, 2015).

The 3-D geometric models produced with GemPy (*de la Varga et al.*, 2019) show a reopening of the syncline to the eastern end (Figure 9). Two explanations are possible: a) strain decreases again to the east, b) slice MOL 1 and the Hausham Syncline plunge towards the west (Figure 1) and thus, in the eastern part only the sole of the syncline is outcropping while the steeper limbs are eroded. Both options are valid, and they are not mutually exclusive.

6.1.2 Along-Strike Geometries of the Kirchbichl Thrust

West of the study area, the deformation front (at Kirchbichl Thrust) features a triangle zone (e.g. *Ortner et al.*, 2015), which is not present in the central and eastern part of our study area (Figures 5c, 6c, 7c, and 8). For the westernmost part of our study area, we show that geometry of the deformation front is different compared to the sections east of it (Figure 4). We offer two interpretations of our data. One features a hinterland dipping thrusts geometry (Figure 4a, as comparable to *Paulus* (1981) or *Ortner et al.* (2015)), while the other one features a small triangle zone that might be a continuation of the triangle zone further west (Figure 4b) (*Shipilin et al.*, 2020). The Koenigsdorf-1 well data (*Paulus*, 1963) do not show indications for backthrusting, which is why we favor the hinterland dipping thrusts interpretation. The well is located 500 meters west of the cross-section trace which limits the probability of projection errors. We suggest that the cross-section is located where a triangle zone transitions into a forethrust dominated geometry. The GemPy models show that data uncertainty in the area is so high that none of the models can be preferred. Overall thrusting of the Kirchbichl Thrust in both cases is 2400 m. Further east, movements on this thrust system sum up to 4600 – 5000 meters (Table 1, Figures 5c, 6c, and 7c). This development in shortening is accompanied by geometric changes, namely tapering out of the Ellbach Thrust (e.g., *Ortner et al.*, 2015) and the development of the Kirchbichl Thrust to a four-strands ramp-flat structure without a triangle zone.

6.1.3 Strain Distribution in the Study Area

We report shortening of the Subalpine Molasse of more than 6 kilometers in the central and eastern part of the study area. *Ortner et al.* (2015) obtained 8 kilometers for the same area. This difference is mostly a result of the interpretation of the throw on the Kirchbichl Thrust, as well as the amount of shortening accommodated on the Leitzach Thrust. Shortening by folding with about 2500 meters (1950 m (cross-section (2), 2300 m (cross-section (3), and 2800 m (cross-section (4) for our restoration) (Table 1, Figures 5c, 6c, and 7c) is comparable in both studies.

We obtain much less shortening of only 3500 m for the western part of the study area as compared to the central and eastern part. We measured less shortening for the Kirchbichl Thrust system (2450 m of shortening), only half of shortening by folding of the Miesbach Syncline and the Hausham Syncline and Leitzach and Mühlau Thrusts are absent in the west. The area is located just east of the sinistral Loisach and Achmühl transform faults, which may have accommodated some of the strain. Another possibility is strain transfer to structures which are not well constrained by data, such as the frontal triangle zone. Third, distributed deformation (penetrative strain) along either small-scale faults or grain-scale processes may accommodate strain that cannot be measured in section balancing (see also above). In the west, *Ortner et al.* (2015) indicate a triangular wedge below the Subalpine Molasse much larger as compared to sections further east. This structure is associated with a backthrust at the boundary between slice MOL1 and the Helvetic units to the south. The associated steep basal thrusts of the Helvetic and Rhenodanubian Flysch Thrust Sheets is interpreted based on dip data and the well Bocksleiten (*Schmidt-Thomé*, 1949). Possibly, missing strain within the Subalpine Molasse is taken up by this structure. Similarly, increasing strain within tectonic slice MOL1 to the east by overturning of the Hausham Syncline (Table 1, Figures 5a, 6a, and 7a) might be linked to pinch-out of this triangle structure. In the area of cross-sections 2 - 4, the wedge and the associated back-thrust is not indicated in previous studies. In contrast, hinterland dipping thrusts with a tectonic window of Helvetic units within the Rhenodanubian Flysch thrust sheets are present. This points to more strain in this shallow part including the Subalpine Molasse compared to the west. Overturning of the Hausham Syncline might thus indicate the transition from a dominant wedge below the Subalpine Molasse to dominant strain within hinterland dipping thrusts in the Helvetic and Rhenodanubian Flysch Thrust Sheets and the Subalpine Molasse. In parallel, shortening within tectonic slices MOL2 and MOL3 increases towards the east compared to the westernmost cross-section (1).

6.2 Comparison of Classical Cross-Section Balancing and 3-D Probabilistic Modeling

6.2.1 Pitfalls of Single Models and Power of Combined Approach

Primarily, it must be noted that our study area is well suited for highlighting the strengths and weaknesses of the single approaches, making it possible to take the best of these worlds. In regions where data coverage is much lower, stratigraphy is not well established, or the structural history is less well constrained, initial geometric and kinematic concepts may be flawed. Uncertainty modeling of these models will not resolve the implicit bias, but only provide error estimates of the interpreted cross-sections. Thus, instead of quantifying a full uncertainty of the geometries in the subsurface, the models may suggest we have an apparently accurate knowledge of the interpretation of the subsurface within a small error.

Evaluating the single approaches, cross-section balancing and 3-D geometric modeling are powerful stand-alone tools. Using them in combination with probabilistic modeling on the same datasets revealed that all methods have their own advantages and disadvantages. In addition to uncertainties related to data density and quality, uncertainties also arise from the concepts and assumptions underlying the methods. In the following, we discuss disadvantages of the single methods and show how a combined method reduces the associated uncertainties and sources of possible errors.

In MOVE, cross-sections are constructed by projecting data points onto the cross-section planes. Projection errors grow with increasing distance from the section, as the structures are only cylindrical over distances of some hundred meters in some parts of the study area (Figures 1, 9, 10, and 12), as is already visible in satellite imagery. As indicated by our GemPy models, different interpretations are possible as to how cylindrical the structures are. This shows that data projection needs to be carried out with care, as confusing projection errors with structural features can lead to the interpretation of structures that do not exists. Moreover, standard cross-section balancing leaves a high degree of freedom for conceptual interpretations due to the limited and uncertain input data. This leads to conceptual biases (e.g., *Bond et al.*, 2007; *Butler et al.*, 2018; *Schaaf and Bond*, 2019; *Wilson et al.*, 2019).

GemPy (*de la Varga et al.*, 2019) offers the extension to a 3-D consistent model instead of multiple 2-D models that are typical for cross-section balancing. It consequently uses the data exactly in the place they are measured, meaning no projection biases occur. In this way, the 3-D models can reveal structural interpretation errors that are based on data projections onto the wrong side of a fault, for example.

Interpolation modeling with GemPy only uses the data directly without considering expert knowledge, apart from the definition of the layer sequence. While independent of conceptual biases, this may result in geologically unrealistic model results in places of low data density. GemPy forces the model with the least mathematical errors, which does not need to be geologically meaningful. This may result in unrealistic models, particularly when data density is low. One example of our models is the open hose instead of an overturned syncline (Figure 9a). Furthermore, across faults, the algorithm occasionally links horizons that should be separated by the fault. This is responsible for a pronounced drag fold at the Mühlau Thrust, which is not consistent with maps (compare Figure 10a-c and Figure 1). Another weakness of GemPy is that as of now modeling of finite faults is not implemented, which especially limits probabilistic modeling including faults. Ceasing faults, i.e., decreasing offset to zero, cannot be modeled. Fault branches need to be modeled as single faults that share the same position, i.e., the same data points, until the point of branching. In uncertainty modeling, where precise locations for these points are drawn from normal distributions, these faults would not perfectly overlap anymore and create intersecting single faults that render the single models locally meaningless. We also note some issues with uncertainty modeling method in the way we performed it. In the case of the interpolation function used here (*Lajaunie et al.*, 1997; *de la Varga et al.*, 2019), we can consider the interpolated value of the implicit field at a position x as:

$$M(x) = f(x; k_i, d_j, \alpha_k, \beta_l)$$

where k_i denote the positions of the data points, d_j orientation values (e.g., measured dip direction), α_k parameters of the covariance function (e.g., sill and range), and β_l a partitioning of space (*Wellmann et al.*, 2010). In the approach presented here, we treat k_i and d_j as uncertain parameters and assign probability distributions (Section 4.2.3) to these parameters. It would also be possible to consider uncertainties in α_k and β_l, leading to an even larger space of uncertainties. In our case, we consider the uncertainties in interface positions and orientations as dominant, similar to other recent work in this field (e.g., *Lindsay et al.*, 2012; *Pakyuz-Charrier et al.*, 2018; *Bjorge et al.*, 2022). In addition, it would also be possible to incorporate kriging variance as a measure of interpolation uncertainty in the applied geostatistical approach (*Courrioux et al.*, 2015). However, such an analysis would require an extensive set of orientation measurements, which in turn would require a measurement campaign on its own. In the range of all these considerations, we still regard the main consideration of position and orientation uncertainties as a valuable way to decide on data reliability to draw conclusions about the structural variability.

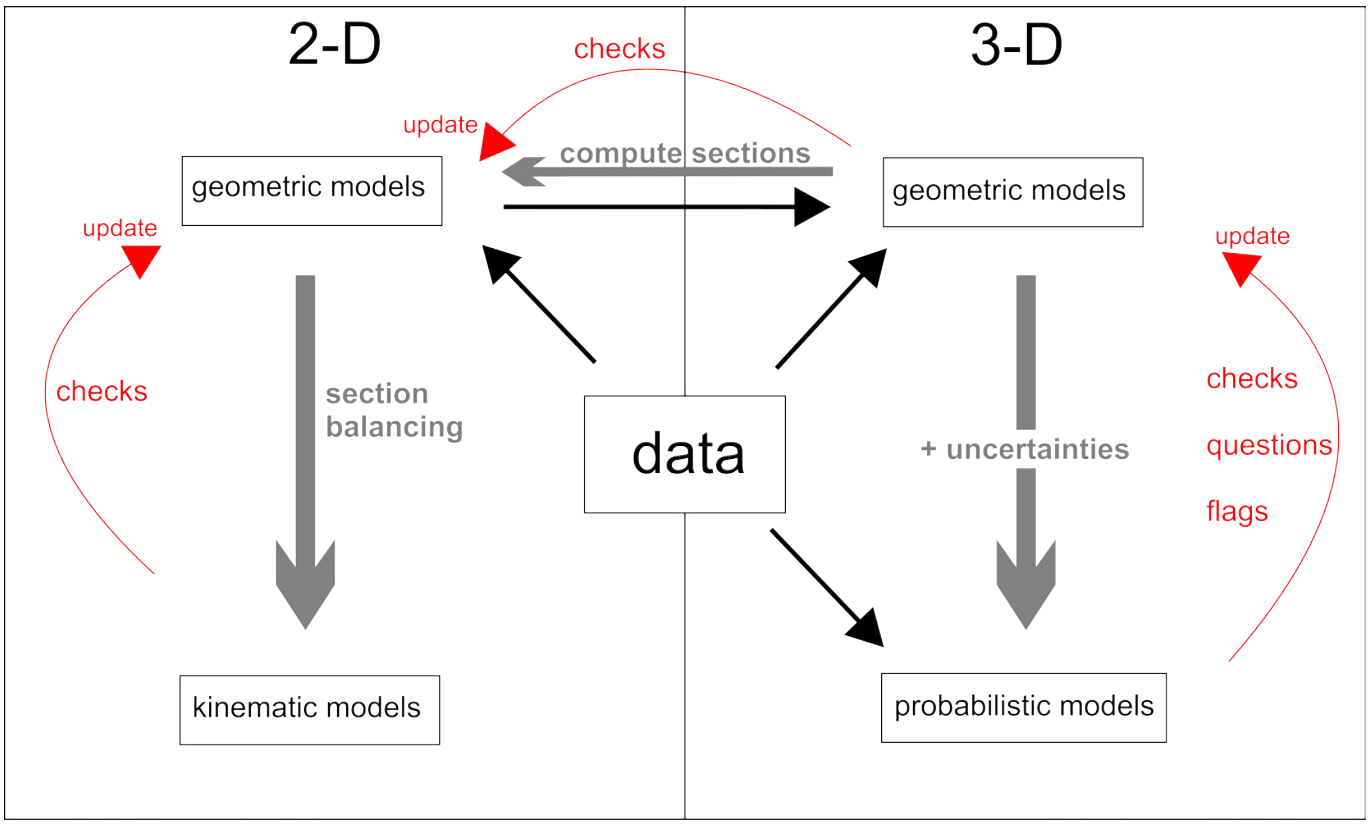

Figure 13 – Proposed combination of the different approaches in an iterative workflow. Black arrows indicate data input. Grey arrows mark modeling steps, where one approach is based on results of the prior method. Red arrows mark control functions that relate the approaches, which are key to establishing an iterative updating process.

A solution to overcome the weaknesses of the individual modeling approaches is their combination and the support by uncertainty modeling. We present the links between the different modeling approaches in Figure 13 and explain their possible integration in an iterative modeling workflow in the following. Data drives all models, while for 2-D models, geometric interpretations in form of cross-sections are produced first. These cross-sections can be kinematically restored by section balancing, which also checks whether the 2-D interpretations kinamatically make sense. In a small iteration circle, the cross-sections can be updated with knowledge from section balancing. Independent from scientist interpretation driven 2-D geometric modeling, GemPy can be used to create 3-D geometric models. Supporting these models, data points generated with geologic knowledge by the interpretation with MOVE (*Petex*, 2018) can be inserted into GemPy. Here, the 3-D models benefit from the extended database, and the consistency of the interpretations made in 2-D interpretational modeling can be evaluated. The lack of kinematic validation of 3-D GemPy models can be solved by computing cross-sections through the 3-D model outputs and balance these in the same manner as the 2-D interpretations. If used in that way, an existing kinematic model can be enhanced with showing where errors exist, also highlighting regions of potential conceptual bias. In the study area such a case is the presence or absence of the triangle zone at depth. While both solutions are possible and can be represented by a kinematic model, 3-D modeling shows that this region is susceptible to bias. This may be of importance if regions of high uncertainty are located in target regions for example in geothermal exploration or nuclear waste storage.

As another addition, probabilistic 3-D modeling based on the data accounts for data uncertainties and quantifies their impact on the structural models. Probabilistic modeling checks plausibility of 3-D geometric models, questions whether models different from the chosen interpretation are possible, and flags volumes of high structural uncertainty. If this step is carried out including data-points generated by geologic interpretation, the impact of these on model entropies can be evaluated.

In summary, 2-D and 3-D geometric modeling as well as kinematic and probabilistic modeling can be integrated into an iterative workflow (Figure 13). The data is used to build independent 2-D interpretational models and 3-D geometric GemPy models. The 2-D model can be tested with section balancing and updated subsequently. Data taken from these cross-sections can be added to the 3-D geometric models computed by GemPy, where useful. This creates an update of the 3-D model and 3-D plausibility of 2-D interpretations can be tested. Probabilistic modeling on the 3-D raw data can highlight volumes where different structural solutions may coexist and where additional data

would help the models. Probabilistic modeling on updated 3-D models shows how additional data modifies uncertainties and cross-checks the added points. Our study shows how the quantification of geometric probabilities reveals where competing geometric solutions exist and shows where uncertainties are highest (Figures 11 and 12). This information can then be used further to reconsider alternative interpretations and point to areas where re-evaluation of data and acquisition of additional data results in reduction of uncertainties and consequently improves model robustness. This approach can be redone iteratively, reducing uncertainties with every step.

6.2.2 Application of the Fully Iterative Approach

In this paper, we show that iterative solving of model problems works for the 3-D shape of the Hausham Syncline, where unsupervised 3-D geometric modeling produces a geologically not reasonable hose structure (Figure 9a). Additionally, probabilistic modeling stresses that in this specific volume, the data allows for two different comparably probable solutions (Figures 11 and 12), which guides to the places where additional data can improve the models. With adding data from iteratively kinematically validated and updated 2-D cross-sections (Figures 5, 6, and 7), this problem can be solved. This is done, again, by an iterative approach of adding such data and updating the 3-D model (Figure 9b).

However, for models including all tectonic slices of the study area, we only present parts of such a fully iterative workflow. This is mainly because at the time of writing, the GemPy software opposes some limitations to fully resolve key volumes. Especially, finite faults, i.e., faults that end at another fault or fault branches cannot be modeled properly. These limitations make it impossible to fully resolve for example the critical volume affected by the Kirchbichl Thrust. The complete iterative workflow can be performed once the needed implementations for our practical field example have been integrated to GemPy. However, with this paper, we already pave the way towards such an iterative workflow and show parts of this cycle, including a 3-D model educated by kinematically validated 2-D geometric interpretation and quantification of uncertainties.

7 Conclusions

We show that combining 2-D cross-section balancing and 3-D steady state modeling makes use of the advantages of both methods and reduces respective shortcomings. In this way, more robust models can be obtained. This paves the way towards a fully iterative approach, fully integrating kinematic, geometric and probabilistic modeling. The latter quantifies uncertainties of the model, providing a quantitative measure for the robustness of geometric constraints and guides towards model volumes of increased uncertainties. This information can either be used to precisely plan additional data acquisition campaigns or motivate to reprocess and reinterpret available data.

Testing elements of this approach, we derive constraints for the architecture of the Hausham Syncline area of the Subalpine Molasse. The Hausham Syncline overturns progressively towards the east. 3-D probabilistic modeling shows that strike-slip faults are not needed to explain this change in geometry. The geometric change of the Hausham Syncline implies either that it accommodated more strain in the east, or is simply a result of outcrop conditions due to the plunge of the fold axis. Additional strain in parts of the anticline could be compensated by less strain below the Syncline in this part compared to a wedge of Helvetic and Ultrahelvetic units farther west. While the Syncline is moved piggyback of this structure in the west, it takes up the strain in the east. Based on existing data it is not possible to distinguish between these two solutions. Likewise, the exact termination of the triangle zone in the west of the study area cannot be determined based on existing data. This structure tapers out in the westernmost part of the study area, with a small remnant of this structure being present at maximum. The suggested modeling approach could show this for both cases, highlighting the importance and feasibility of providing multiple viable solutions when possible.

Acknowledgements

This work is funded by DFG FB-4D project (HA 7660/3-1) within the 4DMD priority program (http://www.spp-mountainbuilding.de). We thank Thomas Fritzer and Jürgen Gruber of the LfU Bavaria for their quick help in providing subsurface data. N. Eichelberger and F. Robledo Carvajal are thanked for constructive reviews, Laura Federico, Adam Forte, Robin Lacassin, and Mohamed Gouiza are thanked for additional comments and editorial handling.

Author contributions

KF: field work, 3-D modeling, probabilistic and kinematic modeling **CvH**: conceived the study, field work **FW**, **EH**, **MV**: 3-D modeling and probabilistic modeling **HO**: field work, kinematic modeling. All authors contributed to discussions. **KF** and **CvH** wrote the manuscript with input from all authors. This study is part of the FB-4D project funded by DFG, granted to **CvH** & **EL**.

Data availability

Data used in this work can be found at: https://doi.org/10.18154/RWTH-2023-08505

Competing interests

The authors declare no competing interests.

Peer review

This publication was peer-reviewed by F. Robledo Carvajal and Nathan Eichelberger. The full peer-review report can be found here: tektonika.online/index.php/home/article/view/21/37.

Copyright notice

References

Ailleres, L., M. Jessell, E. de Kemp, G. Caumon, F. Wellmann, L. Grose, R. Armit, M. Lindsay, J. Giraud, B. Brodaric, M. Harrison, and G. Courrioux (2019), Loop - enabling 3D stochastic geological modelling, in *ASEG Extended Abstracts*, pp. 1–3, Taylor & Francis, doi: 10.1080/22020586.2019.12072955.

Berge, T. B., and S. L. Veal (2005), Structure of the alpine foreland, *Tectonics*, *24*(5), TC5011, doi: 10.1029/2003TC001588.

Bjorge, M., P. Kreye, E. Heim, F. Wellmann, and W. Rühaak (2022), The role of geological models and uncertainties in safety assessments, *Environmental Earth Sciences*, *81*(7), 190, doi: 10.1007/s12665-022-10305-z.

Bond, C. E., A. D. Gibbs, Z. K. Shipton, and S. Jones (2007), What do you think this is? "conceptual uncertainty" in geoscience interpretation, *GSA today: a publication of the Geological Society of America*, *17*(11), 4, doi: 10.1130/gsat01711a.1.

Boyer, S. E., and D. Elliott (1982), Thrust systems, *AAPG bulletin*, *66*, doi: 10.1306/03b5a77d-16d1-11d7-8645000102c1865d.

Brisson, S., F. Wellmann, N. Chudalla, J. von Harten, and C. von Hagke (2023), Estimating uncertainties in 3-D models of complex fold-and-thrust belts: A case study of the eastern alps triangle zone, *Applied Computing and Geosciences*, *18*, 100,115, doi: 10.1016/j.acags.2023.100115.

Burberry, C. M. (2015), Spatial and temporal variation in penetrative strain during compression: Insights from analog models, *Lithosphere*, *7*(6), 611–624, doi: 10.1130/L454.1.

Burkhard, M., and A. Sommaruga (1998), Evolution of the western swiss molasse basin: structural relations with the alps and the jura belt, *Geological Society, London, Special Publications*, *134*(1), 279–298, doi: 10.1144/GSL.SP.1998.134.01.13.

Butler, R. W. H., C. E. Bond, M. A. Cooper, and H. Watkins (2018), Interpreting structural geometry in fold-thrust belts: Why style matters, *Journal of Structural Geology*, *114*, 251–273, doi: 10.1016/j.jsg.2018.06.019.

Courrioux, G., B. Bourgine, A. Guillen, C. Allanic, T. Baudin, F. Lacquement, S. Gabalda, F. Cagnard, B. le Bayon, J. Besse, D. Marquer, P. Trap, P. H. Leloup, and D. Schreiber (2015), Comparisons from multiple realizations of a geological model: implication for uncertainty factors identification, in *17th Annual Conference of the International Association for Mathematical Geosciences–IAMG 2015*, pp. 59–66.

Coward, M. P., and R. W. H. Butler (1985), Thrust tectonics and the deep structure of the Pakistan Himalaya, *Geology*, *13*(6), 417–420, doi: 10.1130/0091-7613(1985)13<417:TTATDS>2.0.CO;2.

Dahlstrom, C. D. A. (1969), Balanced cross sections, *Canadian journal of earth sciences*, *6*(4), 743–757, doi: 10.1139/e69-069.

de la Varga, M., and J. F. Wellmann (2016), Structural geologic modeling as an inference problem: A bayesian perspective, *Interpretation*, *4*(3), SM1–SM16, doi: 10.1190/int-2015-0188.1.

de la Varga, M., A. Schaaf, and F. Wellmann (2019), GemPy 1.0: open-source stochastic geological modeling and inversion, *Geoscientific model development*, *12*(1), 1–32, doi: 10.5194/gmd-12-1-2019.

Freudenberger, W., and K. Schwerd (1996), *Geologische Karte von Bayern, 1:500 000*, 4 ed., Bayrisches Geologisches Landesamt, München.

Frisch, W. (1979), Tectonic progradation and plate tectonic evolution of the alps, *Tectonophysics*, *60*(3-4), 121–139, doi: 10.1016/0040-1951(79)90155-0.

Ganss, O., and P. Schmidt-Thomé (1953), Querprofilserie durch die subalpine molassezone zwischen bodensee und salzach, *Zeitschr. d. dt. Geol. Ges.*, *105*.

Ganss, O., and P. Schmidt-Thomé (1955), Die gefaltete molasse am alpenrand zwischen bodensee und salzach, *Zeitschr. d. dt. Geol. Ges.*, *105*, 402–495.

Gibbs, A. D. (1983), Balanced cross-section construction from seismic sections in areas of extensional tectonics, *Journal of Structural Geology*, *5*(2), 153–160, doi: 10.1016/0191-8141(83)90040-8.

Groshong, R. H. (1975), Strain, fractures, and pressure solution in natural single-layer folds, *GSA Bulletin*, *86*(10), 1363–1376, doi: 10.1130/0016-7606(1975)86<1363:SFAPSI>2.0.CO;2.

Hesse, R. (1982), Cretaceous-Palaeogene flysch zone of the east alps and carpathians: identification and plate-tectonic significance of 'dormant' and 'active' deep-sea trenches in the Alpine-Carpathian arc, *Geological Society, London, Special Publications*, *10*(1), 471–494, doi: 10.1144/GSL.SP.1982.010.01.32.

Hillier, M., F. Wellmann, B. Brodaric, E. de Kemp, and E. Schetselaar (2021), Three-Dimensional structural geological modeling using graph neural networks, *Mathematical geosciences*, *53*(8), 1725–1749, doi: 10.1007/s11004-021-09945-x.

Hillier, M. J., E. M. Schetselaar, E. A. de Kemp, and G. Perron (2014), Three-Dimensional modelling of geological surfaces using generalized interpolation with radial basis functions, *Mathematical geosciences*, *46*(8), 931–953, doi: 10.1007/s11004-014-9540-3.

Jarvis, A., H. I. Reuter, A. Nelson, and E. Guevara (2008), Hole-filled seamless SRTM data V4.

Jessell, M. (2001), Three-dimensional geological modelling of potential-field data, *Computers & geosciences*, *27*(4),

455–465, doi: 10.1016/S0098-3004(00)00142-4.

Jessell, M. W., L. Ailleres, and E. A. de Kemp (2010), Towards an integrated inversion of geoscientific data: What price of geology?, *Tectonophysics*, *490*(3), 294–306, doi: 10.1016/j.tecto.2010.05.020.

Judge, P. A., and R. W. Allmendinger (2011), Assessing uncertainties in balanced cross sections, *Journal of Structural Geology*, *33*(4), 458–467, doi: 10.1016/j.jsg.2011.01.006.

Kley, J., and C. R. Monaldi (1998), Tectonic shortening and crustal thickness in the central andes: How good is the correlation?, *Geology*, *26*(8), 723–726, doi: 10.1130/0091-7613(1998)026<0723:TSACTI>2.3.CO;2.

Kuhlemann, J., and O. Kempf (2002), Post-Eocene evolution of the north alpine foreland basin and its response to alpine tectonics, *Sedimentary geology*, *152*, 45–78.

Lajaunie, C., G. Courrioux, and L. Manuel (1997), Foliation fields and 3D cartography in geology: Principles of a method based on potential interpolation, *Mathematical geology*, *29*(4), 571–584, doi: 10.1007/BF02775087.

Laurent, G., L. Ailleres, L. Grose, G. Caumon, M. Jessell, and R. Armit (2016), Implicit modeling of folds and overprinting deformation, *Earth and planetary science letters*, *456*, 26–38, doi: 10.1016/j.epsl.2016.09.040.

Lindsay, M. W. Jessell, L. Ailleres, S. Perrouty, E. de Kemp, and P. G. Betts (2013), Geodiversity: Exploration of 3D geological model space, *Tectonophysics*, *594*, 27–37, doi: 10.1016/j.tecto.2013.03.013.

Lindsay, M. D., L. Aillères, M. W. Jessell, E. A. de Kemp, and P. G. Betts (2012), Locating and quantifying geological uncertainty in three-dimensional models: Analysis of the gippsland basin, southeastern australia, *Tectonophysics*, *546-547*, 10–27, doi: 10.1016/j.tecto.2012.04.007.

Mallet, J.-L. (1992), Discrete smooth interpolation in geometric modelling, *Computer-aided design and applications*, *24*(4), 178–191, doi: 10.1016/0010-4485(92)90054-E.

Mallet, J.-L. (2004), Space–Time mathematical framework for sedimentary geology, *Mathematical geology*, *36*(1), 1–32, doi: 10.1023/B:MATG.0000016228.75495.7c.

Mayoraz, R., C. E. Mann, and A. Parriaux (1992), Three-dimensional modeling of complex geological structures: New development tools for creating 3-D volumes, in *Computer Modeling of Geologic Surfaces and Volumes*, vol. 96, edited by D. E. Hamilton and T. A. Jones, pp. 261–271, AAPG Special Volumes, doi: https://doi.org/10.1306/CA1564C19.

Mock, S., C. von Hagke, F. Schlunegger, I. Dunkl, and M. Herwegh (2020), Long-wavelength late-miocene thrusting in the north alpine foreland: implications for late orogenic processes, *Solid earth*, *11*(5), 1823–1847, doi: 10.5194/se-11-1823-2020.

Müller, M. (1975), Bohrung miesbach 1: Ergebnisse der ersten im rahmen des erdgastiefenaufschlußprogramms der bundesregierung mit offentlichen mitteln geförderten erdgastiefbohrung, *Compendium*, *75/76*, 63–67.

Oncken, O., C. von Winterfeld, and U. Dittmar (1999), Accretion of a rifted passive margin: The late paleozoic rhenohercynian fold and thrust belt (middle european variscides), *Tectonics*, *18*(1), 75–91, doi: 10.1029/98tc02763.

Oncken, O., D. Hindle, J. Kley, K. Elger, P. Victor, and K. Schemmann (2006), Deformation of the central andean upper plate system - facts, friction, and constraints for plateau models, in *The Andes*, edited by O. Oncken, G. Chong, P. Giese, H.-J. Götze, V. Ramos, M. Strecker, and P. Wigger, pp. 3–27, Springer, Berlin, Heidelberg.

Ortner, H., S. Aichholzer, M. Zerlauth, R. Pilser, and B. Fügenschuh (2015), Geometry, amount, and sequence of thrusting in the subalpine molasse of western austria and southern germany, european alps, *Tectonics*, *34*(1), 1–30, doi: 10.1002/2014TC003550.

Ortner, H., C. Von Hagke, A. Sommaruga, S. Mock, J. Mosar, R. Hinsch, and A. Beidinger (2023), The northern deformation front of the european alps, in *Geodynamics of the Alps - Collisional Processes*, vol. 3, edited by C. L. Rosenberg and N. Bellahsen, pp. 241–312, ISTE-Wiley editions.

Ostheimer, S., and A. Schröder (2016), Geologische karte von bayern 1:25.000, 8235 bad tölz.

Pakyuz-Charrier, E., M. Lindsay, V. Ogarko, J. Giraud, and M. Jessell (2018), Monte carlo simulation for uncertainty estimation on structural data in implicit 3-D geological modeling, a guide for disturbance distribution selection and parameterization, *Solid earth*, *9*(2), 385–402, doi: 10.5194/se-9-385-2018.

Paulus, B. (1963), Zur stratigraphie und fazies der oligozänen und miozänen molasse im südlichen oberbayern, *Bulletin der Vereinigung Schweiz. Petroleum-Geologen und -Ingenieure*, *30*(78), 53–97, doi: 10.5169/SEALS-192671.

Paulus, B. (1981), A revision of the geological section of the tölz-1 wildcat, and evidence of the so far unknown kirchsee syncline at the northern edge of the folded molasse between the isar and mangfall rivers, *Zeitschrift der Deutschen Geologischen Gesellschaft*, *132*(1), 253–276, doi: 10.1127/zdgg/132/1981/253.

Petex (2018), MOVE suite, structural geology modelling software.

Pfiffner, O. A. (1986), Evolution of the north alpine foreland basin in the central alps, in *Foreland Basins*, pp. 219–228, Blackwell Publishing Ltd., Oxford, UK, doi: 10.1002/9781444303810.ch11.

Pflaumann, U., and W. Stephan (1968), Geologische karte von bayern 1:25.000, 8237 miesbach.

Risch, H. (1993), Mikrobiostratigraphische untersuchung an spülproben der bohrung miesbach I, *Geologica Bavarica*, *97*, 125–134.

Schaaf, A., and C. E. Bond (2019), Quantification of uncertainty in 3-D seismic interpretation: implications for deterministic and stochastic geomodeling and machine learning, *Solid earth*, *10*(4), 1049–1061, doi: 10.5194/se-10-1049-2019.

Schmidt-Thomé, P. (1949), Neuere kenntnisse über die kalkalpenzone und die alpenrandstrukturen in südbayern, *Geologische Rundschau: Zeitschrift fur allgemeine Geologie*, *37*(1), 18–24, doi: 10.1007/bf01792492.

Schmitz, M. (1994), A balanced model of the southern central andes, *Tectonics*, *13*(2), 484–492, doi: 10.1029/93TC02232.

Schneeberger, R., M. de La Varga, D. Egli, A. Berger, F. Kober, F. Wellmann, and M. Herwegh (2017), Methods and uncertainty estimations of 3-D structural modelling in crystalline rocks: a case study, *Solid earth*, *8*(5), 987–1002,

doi: 10.5194/se-8-987-2017.

Shipilin, V., D. C. Tanner, H. von Hartmann, and I. Moeck (2020), Multiphase, decoupled faulting in the southern german molasse basin – evidence from 3-D seismic data, *Solid earth*, *11*(6), 2097–2117, doi: 10.5194/se-11-2097-2020.

Sinclair, H. D. (1997a), Tectonostratigraphic model for underfilled peripheral foreland basins: An alpine perspective, *GSA Bulletin*, *109*(3), 324–346.

Sinclair, H. D. (1997b), Flysch to molasse transition in peripheral foreland basins: The role of the passive margin versus slab breakoff, *Geology*, *25*(12), 1123, doi: 10.1130/0091-7613(1997)025<1123:ftmtip>2.3.co;2.

Stephan, W., and R. Hesse (1966), Geologische karte von bayern 1:25.000, 8236 tegernsee.

Stg (2016), *Stratigraphic Table of Germany 2016*, German Research Centre for Geosciences, Potsdam.

Suppe, J., and Y. L. Chang (1983), Kink method applied to structural interpretation of seismic sections, western taiwan, *Petroleum Geology of Taiwan*, *19*, 29–49.

Thiele, S. T., M. W. Jessell, M. Lindsay, V. Ogarko, J. F. Wellmann, and E. Pakyuz-Charrier (2016), The topology of geology 1: Topological analysis, *Journal of Structural Geology*, *91*, 27–38, doi: 10.1016/j.jsg.2016.08.009.

Thomas, R., K. Schwerd, K. Bram, and J. Fertig (2006), Shallow high-resolution seismics and reprocessing of industry profiles in southern bavaria: The molasse and the northern alpine front, *Tectonophysics*, *414*(1), 87–96, doi: 10.1016/j.tecto.2005.10.025.

Tipper, J. C. (1992), Surface modeling for sedimentary basin simulation, in *Computer Modeling of Geologic Surfaces and Volumes*, vol. 96, edited by D. E. Hamilton and T. A. Jones, pp. 93–103, AAPG Special Volumes, doi: 10.1306/CA1564C8.

Turner, A. K. (2006), Challenges and trends for geological modelling and visualisation, *Bulletin of Engineering Geology and the Environment*, *65*(2), 109–127, doi: 10.1007/s10064-005-0015-0.

von Hagke, C., and A. Malz (2018), Triangle zones – geometry, kinematics, mechanics, and the need for appreciation of uncertainties, *Earth-Science Reviews*, *177*, 24–42, doi: 10.1016/j.earscirev.2017.11.003.

von Hagke, C., C. E. Cederbom, O. Oncken, D. F. Stöckli, M. K. Rahn, and F. Schlunegger (2012), Linking the northern alps with their foreland: The latest exhumation history resolved by low-temperature thermochronology, *Tectonics*, *31*(5), TC5010, doi: 10.1029/2011TC003078.

von Hagke, C., O. Oncken, H. Ortner, C. E. Cederbom, and S. Aichholzer (2014), Late miocene to present deformation and erosion of the central alps — evidence for steady state mountain building from thermokinematic data, *Tectonophysics*, *632*, 250–260, doi: 10.1016/j.tecto.2014.06.021.

Wellmann, F., and G. Caumon (2018), 3-D structural geological models: Concepts, methods, and uncertainties, in *Advances in Geophysics*, vol. 59, edited by C. Schmelzbach, pp. 1–121, Elsevier, London, doi: 10.1016/bs.agph.2018.09.001.

Wellmann, J. F., and K. Regenauer-Lieb (2012), Uncertainties have a meaning: Information entropy as a quality measure for 3-D geological models, *Tectonophysics*, *526-529*, 207–216, doi: 10.1016/j.tecto.2011.05.001.

Wellmann, J. F., F. G. Horowitz, E. Schill, and K. Regenauer-Lieb (2010), Towards incorporating uncertainty of structural data in 3D geological inversion, *Tectonophysics*, *490*(3), 141–151, doi: 10.1016/j.tecto.2010.04.022.

Wellmann, J. F., M. Lindsay, J. Poh, and M. Jessell (2014), Validating 3-D structural models with geological knowledge for improved uncertainty evaluations, *Energy Procedia*, *59*, 374–381, doi: 10.1016/j.egypro.2014.10.391.

Wellmann, J. F., M. de la Varga, R. E. Murdie, K. Gessner, and M. Jessell (2018), Uncertainty estimation for a geological model of the sandstone greenstone belt, western australia – insights from integrated geological and geophysical inversion in a bayesian inference framework, in *Characterization of Ore-Forming Systems from Geological, Geochemical and Geophysical Studies*, edited by K. Gessner, T. G. Blenkinsop, and P. Sorjonen-Ward, Special Publications, London, doi: 10.6084/M9.FIGSHARE.C.3899719.

Wilson, C. G., C. E. Bond, and T. F. Shipley (2019), How can geologic decision-making under uncertainty be improved?, *Solid earth*, *10*(5), 1469–1488, doi: 10.5194/se-10-1469-2019.

Witte, J., and O. Oncken (2020), Uncertainty quantification in section-balancing using Pseudo-3D forward modeling – example of the malargüe anticline, argentina, *Journal of Structural Geology*, *141*, 104,189, doi: 10.1016/j.jsg.2020.104189.

Wojtal, S. (1989), Measuring displacement gradients and strains in faulted rocks, *Journal of Structural Geology*, *11*(6), 669–678, doi: 10.1016/0191-8141(89)90003-5.

Woodward, N. B., S. E. Boyer, and J. Suppe (1989), Balanced geological cross-sections, *Short course in geology*, *6*, 132.